Personal Copy
Boyer E.
20"

RM E54C26

NACA RM E54C26

# NACA

# RESEARCH MEMORANDUM

## EXPERIMENTAL INVESTIGATION OF AN AXIAL-FLOW COMPRESSOR INLET STAGE OPERATING AT TRANSONIC RELATIVE INLET MACH NUMBERS

## IV - STAGE AND BLADE-ROW PERFORMANCE OF STAGE WITH AXIAL-DISCHARGE STATORS

By Donald M. Sandercock, Seymour Lieblein, and Francis C. Schwenk

Lewis Flight Propulsion Laboratory
Cleveland, Ohio

NATIONAL ADVISORY COMMITTEE
FOR AERONAUTICS
WASHINGTON

June 28, 1954
Declassified October 31, 1958

NATIONAL ADVISORY COMMITTEE FOR AERONAUTICS

RESEARCH MEMORANDUM

# EXPERIMENTAL INVESTIGATION OF AN AXIAL-FLOW COMPRESSOR INLET STAGE OPERATING AT TRANSONIC RELATIVE INLET MACH NUMBERS

## IV - STAGE AND BLADE-ROW PERFORMANCE OF STAGE WITH AXIAL-DISCHARGE STATORS

By Donald M. Sandercock, Seymour Lieblein, and
Francis C. Schwenk

## SUMMARY

Inasmuch as transonic rotor operation need not necessarily be restricted to the inlet stage, an investigation was conducted to determine the performance characteristics of a transonic stage designed to produce transonic inlet Mach numbers relative to a succeeding stage. The experimental stage was composed of the original transonic rotor reported previously in earlier phases of this investigation and a set of high-turning stator blades. The compounding of transonic stages requires turning of the air back to approximately the axial direction by the stator row. To achieve axial discharge flow, the necessary stator-blade turning for this investigation was approximately 40°. Blade-element performance for rotor and stator is presented over a range of tip speed from 600 to 1100 feet per second. Blade-element performance parameters shown as variations with incidence angle are loss coefficient, deviation angle, inlet Mach number, work coefficient, diffusion factor, efficiency, and axial-velocity ratio. Mass-averaged rotor and stage performance are also included.

Results of the tests showed that if stator blades are set at the minimum-loss incidence angle and if the stator diffusion factor is maintained at moderate values, highly cambered stators can be designed with practically no sacrifice in stage efficiency at the rotor design point compared with conventional low-turning stators. Analysis of the rotor performance at the overspeed condition of 1100 feet per second indicated that shock losses in the tip region of the rotor at peak efficiency do not appear to be significant at a relative inlet Mach number of 1.15.

## INTRODUCTION

Results of recent investigations (refs. 1 to 4) have shown that axial-flow compressor rotors and stages of high efficiency, high pressure

ratio, and high specific mass flow can be obtained by designing for operation in the transonic region of rotor relative inlet Mach number (approximately 1.1 at rotor tip). References 1 and 2 in particular have presented the performance of an inlet stage with a transonic rotor and conventional subsonic stators. The stators in this design had a comparatively low camber angle and produced inlet Mach numbers of conventional magnitudes (up to approximately 0.75) relative to a succeeding rotor row. The good performance obtained from this stage indicated the feasibility of matching a transonic inlet stage with stages of conventional design for multistage application.

In view of the initial success of the transonic inlet stage, it was speculated that transonic operation need not necessarily be restricted to the inlet stage of a multistage unit. Further increases in average stage pressure ratio might be obtained without sacrifice of efficiency if several of the early stages of a multistage compressor were designed for higher than conventional levels of relative inlet Mach number. Thus, a design might involve a gradual transition from the transonic inlet Mach numbers of the inlet stage to the lower Mach number levels of the later stages.

In order to maintain high relative inlet Mach numbers in succeeding rotor rows without markedly increasing the axial velocity across the stage, it is necessary to reduce the amount of absolute rotation (stator-outlet tangential velocity) at the entrance to these rotors. For high-pressure-ratio rotors in particular, this consideration would require stators with considerably greater magnitude of turning angle than currently used. It was thought desirable, therefore, to conduct a further investigation of the original transonic rotor of reference 1 with a set of high-turning stators designed to return the outlet air to the axial direction. For this rotor a stator turning angle of approximately $40^{\circ}$ would be required at design speed. The performance characteristics of a transonic inlet stage designed specifically for operation with succeeding stages of high Mach number level could thus be obtained.

The modified transonic inlet stage with highly turned axial-discharge stators was installed and investigated in a variable-component test rig as in reference 1. The stage and blade-element performance were determined at several tip speeds from 60 to 110 percent of design speed and are presented herein.

## SYMBOLS

Figure 1 is an illustration of air and blade angles employed in this report. The following symbols are used:

$A_f$ compressor frontal area based on rotor tip diameter, 1.646 sq ft

$c_p$ specific heat of air at constant pressure, Btu/(lb)($^{\circ}$R)

$c_v$ specific heat of air at constant volume, Btu/(lb)(°R)

D diffusion factor

g acceleration due to gravity, 32.17 ft/sec$^2$

H total enthalpy, $c_p gJT$, sq ft/sec$^2$

i incidence angle, angle between inlet-relative-air-velocity vector and direction of tangent to blade mean line at leading edge, deg

J mechanical equivalent of heat, 778 ft-lb/Btu

K wall boundary-layer blockage factor

M absolute Mach number

M' relative Mach number

P absolute total pressure, lb/sq ft

P' relative total pressure, lb/sq ft

p static pressure, lb/sq ft

r radius measured from axis of rotation, in.

T absolute total temperature, °R

t static temperature, °R

U blade speed, ft/sec

V absolute velocity of air, ft/sec

V' velocity of air relative to blade row, ft/sec

W weight flow of air, lb/sec

$\beta$ absolute air-flow angle measured from axis of rotation, deg

$\beta'$ air-flow angle relative to blade row measured from axis of rotation, deg

$\gamma$ ratio of specific heats for air, $c_p/c_v$, 1.3947

$\gamma^o$ direction of tangent to blade mean camber line at leading or trailing edge, deg

$\Delta$ symbol used to indicate change in quantity

$\delta$ ratio of inlet total pressure to NACA standard total pressure, $P_1/2117$

$\delta^{\circ}$ deviation angle, angle between outlet-relative-air-velocity vector and direction of tangent to blade mean-line angle at trailing edge, deg

$\eta$ adiabatic temperature-rise efficiency

$\theta$ ratio of compressor-inlet total temperature to NACA standard temperature, $T_1/518.6$

$\theta^{\circ}$ air turning angle, change in relative flow angle from inlet to outlet of blade row, deg

$\rho$ static density of air, lb/cu ft

$\sigma$ solidity, ratio of blade chord to blade spacing

$\varphi$ rotor-inlet flow coefficient at mean radius, $V_{z,3}/U_3$

$\bar{\omega}$ relative total-pressure-loss coefficient

Subscripts:

av average

b blade element

f free stream

h hub

id ideal

m mean radius

R rotor

S stator

st standard

t tip

z axial direction

$\theta$ tangential direction

0 total or stagnation conditions

1 depression tank

2 weight-flow measuring station upstream of rotor

3 rotor inlet

4 rotor outlet (stator inlet)

5 stator outlet

6 compressor outlet (discharge measuring station)

## APPARATUS AND PROCEDURE

### Compressor Design

The transonic compressor rotor used in the investigation was the same as the rotor described in references 1 and 2. The stators were designed to turn the flow from the measured direction at the rotor outlet to approximately an axial direction at the stator outlet with an average outlet axial velocity of 680 feet per second. The corresponding relative inlet Mach number near the tip of a succeeding rotor would then be approximately 1.0.

The double circular-arc profile was chosen for the stator blade since references 1 and 5 indicated good performance for this type of blade shape. Consideration of the radial variation of stator-inlet angle and solidity revealed that, in the interests of rapid design and construction, a blade of constant section could be used. The stators were designed for a constant inlet angle of $45^{\circ}$ at design speed and an incidence angle of $4^{\circ}$, as indicated by the results of reference 5 (the detailed stator analysis of ref. 2 was not available at the time of the design). The design equation for camber angle was obtained from a survey of limited compressor data which suggested the empirical relation of turning angle and camber angle

$$\theta^{\circ} = 0.8\varphi + 0.8i \tag{1}$$

With these values, double circular-arc stator blades (circular-arc suction and pressure surfaces) were designed with the following properties constant at all radii:

| | |
|---|---|
| Camber angle, deg | 52 |
| Mean-line chord, in. | 3.20 |
| Maximum thickness | 0.07 × chord length |
| Leading-edge and trailing-edge radii, in. | 0.020 |

At the time of installation it was decided that a more desirable match point would be obtained if the stator blades were set for an inlet angle of 40°. It was subsequently decided to set the blades at the incidence angle of 4° indicated in reference 5 and to accept the overturning due to the excessive camber angle for this condition.

For comparative purposes, it was desirable to keep the design stator diffusion factors (ref. 6) at approximately the same levels as in the low-camber design of reference 2. In order to compensate for the increased diffusion due to the larger change in $V_\theta$, the annulus area across the stators was reduced in order to increase the axial component of velocity to a value of 680 feet per second (equal to the design value of axial velocity at the rotor inlet).

Each suction and pressure surface of all blade-profile sections was a circular arc passing through the maximum-thickness point located at the 50-percent-chord position and tangent to 0.020-inch-radius circles whose centers are placed at the end points of the mean camber line. Rotor- and stator-blade profiles at the hub and tip are shown in figure 2.

## Compressor Installation

The compressor installation is the same as the one described in reference 2 except that a wood fairing was placed around the hub section to obtain the desired decrease in annulus area across the stator row. The fairing had a smoothly curved surface from a radius of 5.30 inches approximately 1 inch ahead of the stator-blade leading edge to a constant radius of 5.95 inches at the stator-blade trailing edge. A sketch of the transonic-compressor test rig is shown in figure 3.

## Instrumentation

Outlet conditions used for computing stage over-all performance were determined at station 6 (3 in. downstream of the stator-blade trailing edge) from 15 individual total-pressure (kiel) probes and 15 iron-constantan thermocouples (three rakes with five thermocouples on each rake similar to the one shown in fig. 4). The total-pressure probes and total-temperature rakes were so oriented that measurements were obtained radially at the centers of five equal areas and circumferentially at three equally spaced positions across the stator passage.

A complete description of the survey instruments, their use, calibration, and location, is given in reference 2 with the following minor exception: At station 5, instead of measuring total pressure by means of fixed wake rakes, a complete radial survey with a 35-tube circumferential wake rake was used to determine the total-pressure field. Twenty-nine of the tubes were spaced 0.050 inch apart in order to obtain an accurate definition of the blade wake. A photograph of the wake rake installed behind the stator blade is shown in figure 5, and photographs of the other probes and instruments used are shown in figure 4.

For surveying purposes, the passage was divided radially into six equal parts. Discounting the inner and outer wall boundaries resulted in five major radial survey positions, all outside the boundary-layer regions, at which blade-element performance is presented. Several radial survey stations within the wall boundary-layer regions at the hub and tip were also included for integration purposes. Total-pressure and angle measurements were observed at all survey positions, whereas static pressures were observed at the five major survey positions only. At stations 4 and 5, respectively, total temperatures were obtained from faired radial variations of total temperature measured by a single six-tip rake (fig. 4) and from the five-tip rakes located at station 6. No temperature probes were installed at station 5.

The same reliability checks applied in reference 2 are used in this report, that is, comparisons between integrated weight flows at the various measuring stations and inlet orifice weight flow, and comparisons between momentum and temperature-rise efficiencies. The following results are presented as checks on the reliability of the data:

(1) For the speeds investigated, the variation between integrated weight flows at any station and that given by the thin-plate orifice was less than 3 percent.

(2) Mass-averaged momentum efficiencies were greater than the mass-averaged temperature-rise efficiencies by approximately 2 percent or less for a tip speed of 600 feet per second and by 3 to 6 percent at tip speeds of 1000 and 1100 feet per second.

## Procedure

The procedure and conditions observed in conducting these tests followed that outlined in reference 1 for the over-all performance and in reference 2 for the survey, or blade-element, performance with one minor exception. For the runs at 110 percent of design speed, refrigerated air was used in order to reduce the actual rotor speed required for the given corrected speed. The average inlet total temperature for these runs varied between 33° and 38° F.

### Computations

The presentation of data and the performance parameters used are identical to those given in reference 2. The equations used in computing the stage and blade-element performance are presented in the appendix and defined more completely in reference 2.

## ROTOR PERFORMANCE

Performance characteristics for this rotor when operating with low-turning stators at tip speeds of 800 and 1000 feet per second were presented in reference 2. The present discussion presents additional detailed data at 600 and 1100 feet per second as well as corroborating data at the design speed of 1000 feet per second. The measurements of rotor performance at design speed were in agreement with the data of reference 2.

### Inlet Conditions

Preliminary surveys of the inlet section indicated that the air entering the rotor row had no prewhirl; and, since no guide vanes were used, the rotor absolute inlet velocity was considered to be axial in direction for all inlet calculations. Figure 6 shows the measured radial variation of inlet absolute Mach number plotted as a ratio of Mach number to mean-radius Mach number. The three weight flows presented represent a point of high weight flow, one near peak efficiency, and a point of low weight flow on each of the constant speed curves. In general, the gradient shows little variation with either speed or weight flow. The radial variation of relative air inlet angle over a range of tip speed and weight flow is shown in figure 7. Blade angles are included in figure 7 to permit an evaluation of the radial variation of incidence angle at the various speeds.

### Blade-Element Characteristics

The significance and origin of the various parameters used in the analysis of rotor-blade-element performance and the use of these parameters are discussed in reference 2. The variation of significant rotor-blade-element characteristics with incidence angle is presented for the five principal radial positions in figure 8 for tip speeds of 600, 1000, and 1100 feet per second. The two end points were about 16 percent of the passage height (0.455 in.) away from the end walls and were outside the wall boundary-layer regions. A summary of the geometry of each rotor-blade element at these survey positions is presented in table I.

2Y

Relative total-pressure-loss coefficient. - The variations of relative total-pressure-loss coefficient (eq. (A4)) with incidence angle shown in figure 8 are typical of airfoil sections in general (e.g., ref. 5). The loss trends which were reported in reference 2 are accented at the additional compressor tip speed of 1100 feet per second. At the tip section, for the higher tip speed (and consequently higher relative inlet Mach number), there is a marked decrease in low-loss range of incidence angle, primarily on the low-incidence side, and an increase in the magnitude of the minimum loss coefficient. In general, these same trends are carried out at each of the sections; however, they are most pronounced at the tip region. With the continual decrease in the low-loss range of incidence angle with increasing Mach number, the determination of the design (minimum-loss) incidence angle requires greater accuracy as the design Mach number is increased.

In the presence of high inlet Mach numbers, an increase in the general loss-coefficient level with an increase in Mach number (or compressor tip speed) may be caused by both an increase in blade loading and by formation of shock waves on the blade surfaces. The relative effects of the increase in loss coefficient due to each factor can be roughly evaluated by means of the diffusion factor of reference 6, as explained in reference 2. Figure 9 presents a plot of relative total-pressure-loss coefficient against diffusion factor for all radial positions. Data for the correlation were obtained from points in the low-loss range of incidence angle in figure 8. Radial position 3 at a radius of 8.300 inches (fig. 9(a)) is also included here since its radial location (11 percent of blade height from the outer wall) permits a comparison with the tip-region data collected in reference 6 (10 to 12 percent of passage height from outer wall). The range of loss-coefficient-against-diffusion-factor data for rotors operating below their limiting Mach numbers (start of strong shock losses) presented in reference 6 is shown by the dashed lines in figure 9(a). The solid symbols in figure 9(a) represent the data points obtained from the same rotor in the low-loss range of incidence angle at a tip speed of 1000 feet per second as reported in reference 2.

From the correlation of figure 9(a), it appears that the increase in the minimum-loss coefficient at a tip speed of 1100 feet per second can still be attributed to an increase in blade loading (as measured by the diffusion factor) and to associated end losses for tip-region relative inlet Mach numbers up to about 1.15. For the remainder of the blade, essentially no trend of variation of loss coefficient with diffusion factor is observed over the range of diffusion factor encountered, which is characteristic of the variations obtained for blade sections in two-dimensional cascade flow. The increased level of loss in the hub region at all speeds (fig. 9(f)) is probably an indication of the hub-region end losses.

Deviation angle. - Although some spread of the data exists over the speed range, figure 8 shows a trend of increasing deviation angle with an increase in tip speed. The trend is especially noticeable at blade elements near the hub and evident to a lesser degree near the blade tip. The variation of deviation angle with tip speed is more logically related to the change in the axial-velocity ratio across the element than to the changes in loss or relative inlet Mach number. Changes in deviation angle with variations in axial-velocity ratio have been demonstrated in reference 7 and other unpublished data.

The radial variation of the slope of the curve of deviation angle against incidence angle for $U_t/\sqrt{\theta} = 600$ feet per second is probably due to the effect of solidity as given by cascade potential-flow considerations. This variation appears to be masked at the higher speeds by the effect of losses on the deviation angle.

At design speed, the higher values of deviation angle at position 8 (near hub) in figure 8 compared with the values of reference 2 may be due to the higher loss level at the radius and possibly to the difference in hub curvature at the rotor outlet.

Turning angles may be computed from the incidence, deviation, and blade-inlet and -outlet angles (table I) from the relation

$$\theta^{\circ} = \gamma_3^{\circ} - \gamma_4^{\circ} + i - \delta^{\circ} \tag{2}$$

Work coefficient. - The actual work coefficient $\Delta H/U_t^2$ (eq. (A8)), a nondimensional temperature-rise parameter used for correlating stage performance over a range of speed, is plotted against incidence angle in figure 8. For a given incidence angle (or given flow coefficient), the work coefficient does not vary with tip speed as long as geometrically similar velocity triangles are maintained. The condition of geometric similarity is generally satisfied if the turning angles and the ratio of outlet to inlet axial velocity remain constant over the speed range. For the tip speeds investigated, the data of figure 8 show a small decrease in turning angle and a substantial decrease in axial-velocity ratio across the blade row as speed is increased. The variation in axial-velocity ratio with tip speed is about the same at all radial positions, but the decrease in turning angle is most pronounced at the hub. The decrease in axial-velocity ratio is due to compressibility effects on density at high levels of pressure ratio.

Increases in work coefficient with tip speed are most pronounced in the tip region. As explained in reference 2, this result is due to the effect of a higher value of relative outlet angle at the tip causing a larger change in outlet tangential air velocity $V_\theta$, and therefore in work

input, for a given change in axial-velocity ratio. Near the hub section the changes in deviation angle and axial-velocity ratio have opposite effects; and, furthermore, since the outlet relative angle is smaller, the net effect on the work input is greatly reduced. Thus, the variation in work coefficient with tip speed is considerably reduced in the hub region. These results indicate the critical nature of the flow in the rotor tip region, and careful consideration should be given in the design of tip-region blading and velocity diagrams for high-performance rotors.

Efficiency. - In equation (A7), rotor efficiency is shown to be a function of the relative total-pressure-loss coefficient, the energy input, and the inlet relative Mach number. Consequently, variation with tip speed of the magnitude of the efficiency of an element then depends on the specific individual rates of increase of the various factors involved.

In the tip region of the blade, although the relative inlet Mach number and minimum relative total-pressure-loss coefficient increase markedly with increasing tip speed, the work input is also increasing, and the efficiency tends to be maintained. The principal influencing factor in the tip region for this rotor appears to be the variation of axial-velocity ratio which affects both the work coefficient and the diffusion factor (and therefore the loss). For the range of tip speed investigated, shock losses do not appear to be strong at peak efficiency.

In the central region of the blades, as revealed in figure 8(c), the element efficiency tends to remain essentially constant with tip speed, since the variation with tip speed of both minimum relative total-pressure-loss coefficient and work coefficient is reduced compared with the variation in the tip region. The increase in total work input as speed is increased is apparently sufficient to overcome the effect on efficiency of the increase in relative Mach number (eqs. (A7) and (A8)). At the hub, the efficiency variation is primarily a reflection of the variation of the loss coefficient.

## Outlet Conditions

Rotor-outlet conditions are presented in figure 10 as plots of total-pressure ratio, absolute and relative Mach number, absolute airflow angle, and efficiency against radius for three corrected weight-flow points at each tip speed of 600, 1000, and 1100 feet per second.

The increase in radial gradient of total-pressure ratio at the higher speed levels is a result of the compounding effects of both the magnitude of the wheel speed and the decrease in axial-velocity ratio across the rotor (effect on work coefficient as discussed previously).

A pressure ratio of greater than 1.7 was attained in the tip region at 1100 feet per second. The decrease in the radial gradient of pressure ratio for the high weight-flow point at a corrected rotor tip speed $U_t/\sqrt{\theta}$ of 1100 feet per second is a reflection of the sensitivity of the tip-region pressure ratio to changes in efficiency and axial-velocity ratio at high levels of tip speed (figs. 8(a) and (b)).

Over the main portion of flow, the radial gradients of outlet absolute angle and absolute and relative Mach number show little variation with tip speed and weight flow over the ranges investigated. The radial variations of efficiency clearly indicate the importance of the tip-region efficiency at the higher tip speeds.

Examination of the radial distribution of weight flow for several weight flows at the tip speed of 1100 feet per second (fig. 11), as was done in reference 2, revealed essentially no change in the distribution of the weight flow across the rotor, except for a slight shift toward the center to compensate for the area reduction due to wall boundary-layer growth across the rotor. Approximately half of the rotor-blade span was operating with relative inlet Mach numbers of 1.0 and greater for these runs.

## Averaged Performance

Pressure ratio and efficiency. - Mass-averaged rotor pressure ratio (eq. (A3)) and mass-averaged rotor temperature-rise efficiency (eq. (A2)) are shown in figure 12 plotted against corrected weight flow per unit frontal area. A peak efficiency of about 0.92 and a peak pressure ratio of about 1.5 at design speed ($U_t/\sqrt{\theta}$ = 1000 ft/sec) are indicated. For $U_t/\sqrt{\theta}$ = 1100 feet per second, at which the inlet relative Mach number at the tip varied between approximately 1.19 and 1.14, peak efficiency was approximately 0.905 at a pressure ratio of 1.60 and a specific weight flow of 29.7 pounds per second per square foot. Peak pressure ratio obtained was 1.65. The continued reduction in range of operation as inlet Mach number is increased is apparent.

Wall boundary-layer blockage factor. - The wall boundary-layer blockage factor $K$ is defined as the ratio of the actual weight flow to the ideal weight flow that would exist in the annulus if the free-stream conditions continued out to the walls. Numerical integration was used to compute the actual and ideal weight flows.

At station 2 (upstream of the rotor), the blockage factor $K_2$ varied with weight flow between values of 0.985 and 0.990 (ref. 2). At station 4 (downstream with the rotor), the blockage factor $K_4$ varied with speed as well as with weight flow according to the following table:

| $U_t/\sqrt{\theta}$, ft/sec | $W\sqrt{\theta}/\delta A_f$, lb/(sec)(sq ft) | $K_4$ |
|---|---|---|
| 600 | 15.74 | 0.940 |
| 600 | 18.18 | .950 |
| 600 | 23.37 | .958 |
| 1000 | 25.15 | .940 |
| 1000 | 27.37 | .944 |
| 1000 | 29.14 | .956 |
| 1100 | 27.52 | .940 |
| 1100 | 29.18 | .944 |
| 1100 | 30.14 | .935 |

## STATOR PERFORMANCE

The discussion of stator performance is presented in the same manner as the rotor performance. Stator-inlet conditions are taken from the measured rotor-outlet conditions at station 4. Two additional tip speeds of 800 and 900 feet per second are reported for the stator investigations.

### Blade-Element Characteristics

Blade-element performance is presented at five major radial survey positions equally spaced across the stator-outlet passage. Figures 13(a) to (c) present the basic blade-element characteristics of the stator-blade row. A summary of the stator-blade geometry at the radial positions reported is presented in table II.

Total-pressure-loss coefficient. - The stator loss coefficient is defined (eq. (A5)) as the ratio of the difference between the stator free-stream outlet total pressure and the average outlet total pressure to the difference of the total and static pressures at the stator inlet. The average outlet total pressure was obtained from an area average of the plotted circumferential variation of outlet total pressure. Inasmuch as the measured free-stream total pressures on the pressure and suction sides of the wake were not generally identical, the free-stream value of total pressure used in the calculation was established as an average of all pressure readings in the free stream on both sides of the wake. An example of a circumferential variation of total pressure as measured by the wake rake is shown in figure 14. The magnitudes of the computed values of the loss coefficient are not considered precisely accurate because of the general difficulty of establishing a valid value of the free-stream total pressure. In some cases, particularly at 1100 feet per second, a significant circumferential variation of total pressure was measured in the so-called free-stream flow.

At the lower tip speeds of 600 and 800 feet per second (which corresponds to a variation of stator-inlet Mach number from about 0.40 to 0.60), the tip speed had little effect on the form or magnitude of the loss-coefficient variation with incidence angle. At the higher tip speeds (1000 and 1100 ft/sec) the stator setting was such that within the range of operation of the rotor the region of minimum stator loss could not be determined. However, values obtained on the positive incidence side of the minimum-loss point did not evidence any appreciable variation of loss coefficient with increasing Mach number. This is reasonable, since cascade results for this blade shape (at lower camber) show little variation of loss coefficient with Mach number on the positive incidence side. The range of stator operation is approximately the same as the range for the low-turning circular-arc stator blades at the tip speeds of 800 and 1000 feet per second reported in reference 2.

Except for the hub and tip positions, a minimum value of stator-loss coefficient of about 0.02 is obtained. This is consistent with cascade results for a lower-camber blade (ref. 5) and with the measured values of inlet Mach number and diffusion factor at minimum loss (ref. 6).

The minimum-loss (design) incidence angle appears to be between about $-1^{\circ}$ and $-4^{\circ}$ from hub to tip. In reference 2, the incidence angle for a double circular-arc blade of $20^{\circ}$ camber (same inlet conditions and about same solidity) was found to be about zero. The reduction in design incidence observed for the $52^{\circ}$ camber blade is entirely reasonable, since cascade data and potential theory indicate that design incidence angle decreases with increasing camber (e.g., see ref. 8).

Because of the large difference between actual minimum-loss incidence angle and the original design setting (incidence angle of $+4^{\circ}$), the stators were not very well matched with the rotor at peak rotor efficiency for design tip speed of 1000 feet per second. The measured over-all efficiency is therefore not a true indication of the best efficiency potential of the stage. Unfortunately, time did not permit a resetting of the stators. However, an estimate of the stage performance with properly set stators can be made from the loss curves of figure 13. If the blades had operated at the minimum-loss incidence angle at all sections (resetting the blades to an incidence angle of $-2^{\circ}$ would approximately accomplish this), then the average stator-loss coefficient at the rotor peak efficiency point would have been reduced from about 0.10 to 0.03. This reduction in loss coefficient would have resulted in an increase of 0.02 in stage efficiency and 0.013 in total-pressure ratio.

Deviation angle. - As in reference 2, angle measurements at the stator outlet were taken at only one circumferential position, approximately midway between two blades. In the tip region (fig. 13(a)), a rather pronounced increase in deviation angle with incidence angle is observed. The increase in deviation angle with incidence angle

(as well as the average magnitude of the deviation angle) then becomes progressively smaller toward the hub of the stator where a reverse trend is indicated. No plausible explanation can be advanced for this variation. Although a decrease in the slope of deviation angle against incidence angle is expected as solidity is increased in potential flow, the higher level and the degree of change of solidity from tip to hub of the stator make this solidity effect negligible. Furthermore, there are no large differences in the form of the loss curves from tip to hub. The observed deviation-angle trend with radius may therefore be caused by some secondary-flow effects or by the inability of the single angle reading to accurately represent the average flow direction over the entire range of flow conditions. The influence of the losses on the deviation-angle variation is expected to be greater for the stator than for the rotor because of the greater variation in the magnitude of the stator-loss coefficient over the range of incidence angle investigated.

Inasmuch as the stators were designed with circular-arc mean-line sections, a comparison was made between the measured deviation angles and those computed from Carter's rule for circular-arc elements (ref. 9) given by

$$\delta^{\circ} = m\varphi\sqrt{1/\sigma} \tag{3}$$

where $m$ is a variable depending on blade-chord angle (curve of $m$ values is given in ref. 9). For the three central survey positions in figure 13 (positions 5, 6, and 7), Carter's rule shows good agreement with measured values in the minimum-loss range of incidence angle ($-1^{\circ}$ to $-4^{\circ}$). Near the tip, the deviation rule seems to predict angles too low, while near the hub, calculated deviation angles are too high. It should also be noted that good agreement between observed deviation angles at minimum-loss incidence angle and Carter's rule in the central portion of the blade was also found for the $20^{\circ}$-camber circular-arc stators in reference 2.

## Outlet Conditions

Figure 15 contains several examples of the radial variation of stator-outlet Mach number and air angle for tip speeds of 600, 1000, and 1100 feet per second. The angle measurements were taken from a single probe located midway between two blades. Mach numbers were computed from radially faired static-pressure readings of a single probe surveying the midpassage position between two blades and the circumferentially averaged total-pressure data.

The general overturning of the flow at the stator outlet resulting from the overcambered blade is indicated by the negative angle values. The radial variation of turning angle is a reflection of the large

radial variation of deviation angle. The general increase in the radial gradient of outlet Mach number at the higher tip speeds is a result primarily of the increase of the radial gradient of total energy.

Weight-flow blockage factors at the stator outlet $K_5$ varied with speed and weight flow according to the following table:

| $U_t/\sqrt{\theta}$, ft/sec | $W\sqrt{\theta}/\delta A_f$, lb/(sec)(sq ft) | $K_5$ |
|---|---|---|
| 600 | 15.74 | 0.947 |
| 600 | 18.18 | .939 |
| 600 | 23.37 | .932 |
| 1000 | 25.15 | .956 |
| 1000 | 27.37 | .947 |
| 1000 | 29.14 | .943 |
| 1100 | 27.52 | .955 |
| 1100 | 29.18 | .949 |
| 1100 | 30.14 | .947 |

## STAGE PERFORMANCE

The over-all performance of the stage was determined primarily from area-averaged total-pressure and total-temperature data obtained from the fixed probes located downstream of the stator at station 6. The use of the fixed probes permitted the rapid determination of stage performance over wider ranges of weight flow and tip speed than was covered by the surveys. Mass-averaged stage performance was also obtained from the mass-averaged conditions determined from the surveys at the stator outlet (station 5). Inasmuch as no temperature probes were installed at station 5, temperature data for the mass averages were obtained from faired radial variations of total temperature measured by the five-tip rakes at station 6.

Area- and mass-averaged stage efficiency and pressure ratio are plotted against corrected weight flow per square foot of frontal area in figure 16 over a wide range of tip speed. For comparison and to give some idea of the drop in efficiency across the stators, the mass-averaged rotor-performance characteristics are also included in the figure for tip speeds of 600, 1000, and 1100 feet per second. The good correlation of the stage performance obtained from the two methods indicates the satisfactory nature of the fixed-probe system for measuring over-all performance.

3Y

At design speed, a peak stage efficiency of 88.5 percent was recorded at a corrected specific weight flow of 27.8 pounds per second per square foot of frontal area and a pressure ratio of 1.47. These values occurred at approximately the peak efficiency point of the rotor also. Peak pressure was 1.47 at a corrected specific weight flow of 26.2 pounds per second per square foot.

For the 10 percent overspeed runs (1100 ft/sec), a peak efficiency of 85.8 percent was attained at a pressure ratio of 1.57 and a corrected specific weight flow of 29.5 pounds per second per square foot. Peak pressure ratio recorded at this tip speed of 1100 feet per second was 1.58 at a corrected specific weight flow of 28.4 pounds per second per square foot of frontal area and an efficiency of 0.845.

As discussed in the section Total-pressure-loss coefficient for the stator blades, if, at the peak efficiency point of design speed, the stator blades had been set at their minimum-loss incidence angles at all sections, gains of about 0.02 in efficiency and 0.013 in total-pressure ratio could have been realized. This setting would have raised the stage peak efficiency to approximately 0.90 and stage total-pressure ratio to 1.48. Both these stage performance characteristics compare very favorably with those reported in reference 2 for the same rotor with low-turning stator blades.

In order to generalize the stage performance, the over-all stage work input was computed in the dimensionless form $\Delta H/U_t^2$ which, together with stage over-all efficiency, is plotted against the mean-radius rotor-inlet flow coefficient $(V_{z,3}/U_3)_m$ in figure 17 for the range covered by the survey tests. As was noted for the rotor-blade element (especially at the tip), the area-averaged work coefficient increases with tip speed.

## SUMMARY OF RESULTS

The following results were obtained from the experimental investigation of a transonic compressor stage composed of the transonic rotor of a previous report and a set of axial-discharge high-turning stators operating over a range of tip speed:

Analysis of the rotor performance indicated that:

1. Operation of the rotor at a tip speed of 1100 feet per second, for which the inlet relative Mach number at the tip varied between approximately 1.19 and 1.14, showed an increase in average pressure ratio to 1.60 at peak efficiency and a decrease in average peak rotor efficiency to 0.905 over those values obtained at design speed.

2. Blade-element analysis indicated that at the minimum-loss incidence angle for the tests at a tip speed of 1100 feet per second, the observed increase in the magnitude of the minimum loss in the tip region can be attributed to the effects of increased blade loading. Shock losses appear to be small.

Analysis of the stator-blade-row performance indicated that:

1. Total-pressure-loss characteristics were generally similar to those of similarly shaped stator blades of lower camber reported previously (diffusion factors and inlet Mach numbers were approximately the same).

2. Except at the hub and tip regions, Carter's rule showed good agreement with measured deviation angles at the minimum-loss incidence angles.

3. Incidence angle for minimum stator loss was about $-1^{\circ}$ to $-4^{\circ}$. The stator blades were not set at the best incidence angle for operation with the rotor at peak rotor efficiency.

Analysis of the complete stage indicated that:

1. At design speed (corrected rotor tip speed of 1000 ft/sec), a peak mass-averaged efficiency of 0.885 was attained at a corrected specific weight flow of 27.8 pounds per second per square foot of frontal area and a mass-averaged total-pressure ratio of 1.47.

2. If the stator-blade elements had been set at a minimum-loss incidence angle at rotor peak efficiency (a negative reset of $6^{\circ}$ would approximately have accomplished this), a calculated increase in stage efficiency of 0.02 and in stage total-pressure ratio of 0.013 would have occurred. Thus, the performance characteristics at peak efficiency for design speed (corrected rotor tip speed of 1000 ft/sec) for this stage would have been very close to those observed for this same rotor with a set of similarly shaped low-turning stator blades previously reported.

Lewis Flight Propulsion Laboratory
National Advisory Committee for Aeronautics
Cleveland, Ohio, March 24, 1954

## APPENDIX - PERFORMANCE EQUATIONS

All the equations used in this report are listed here. These equations are developed and discussed in the included references.

1. Blade-element temperature-rise efficiency. By assuming that $P_3 = P_1$ and $T_3 = T_1$,

$$\eta_b = \frac{T_1\left[\left(\frac{P_4}{P_1}\right)^{\frac{\gamma-1}{\gamma}} - 1.0\right]}{T_4 - T_1} \tag{A1}$$

2. Mass-averaged temperature-rise efficiency

$$\eta = \frac{T_1\int_{r_{h,4}}^{r_{t,4}} \rho_4 V_{z,4} r_4 \left[\left(\frac{P_4}{P_1}\right)^{\frac{\gamma-1}{\gamma}} - 1\right] dr_4}{\int_{r_{h,4}}^{r_{t,4}} \rho_4 V_{z,4} r_4 (T_4 - T_1)\, dr_4} \tag{A2}$$

3. Mass-averaged total-pressure ratio

$$\frac{P_4}{P_1} = \left\{\frac{\int_{r_{h,4}}^{r_{t,4}} \left[\left(\frac{P_4}{P_1}\right)^{\frac{\gamma-1}{\gamma}} - 1\right] \rho_4 V_{z,4} r_4 dr_4}{\int_{r_{h,4}}^{r_{t,4}} \rho_4 V_{z,4} r_4 dr_4} + 1.0\right\}^{\frac{\gamma}{\gamma-1}} \tag{A3}$$

4. Rotor relative total-pressure-loss coefficient (ref. 6)

$$\bar{\omega}_R = (P_4'/P_3')_{id} \times \left[\frac{1 - \left(\frac{P_4}{P_3}\right)\left(\frac{T_4}{T_3}\right)^{-\frac{\gamma}{\gamma-1}}}{1 - \left(1 + \frac{\gamma-1}{2} M_3'^2\right)^{-\frac{\gamma}{\gamma-1}}}\right] \tag{A4}$$

where $(P_4'/P_3')_{id}$ was taken equal to 1 for all computations used herein.

5. Stator wake total-pressure-loss coefficient (ref. 6)

$$\bar{\omega}_S = (P_{5,f} - P_{5,av})/(P_4 - p_4) \tag{A5}$$

6. Area-averaged stage efficiency

$$\eta = T_1\left[\frac{\sum_{n=1}^{5}\left(\frac{P_5}{P_1}\right)_n^{\frac{\gamma-1}{\gamma}} - 1}{\sum_{n=1}^{5}(T_6 - T_1)_n}\right] \tag{A6}$$

where $T_5 = T_6$ and $n$ refers to the readings at the centers of the five equal areas at which the instruments were placed.

7. Rotor blade-element efficiency in terms of loss coefficient (ref. 2)

$$\eta_b = \frac{\frac{T_4}{T_3}\left\{1.0 - \bar{\omega}_R\left[1.0 - \left(1.0 + \frac{\gamma-1}{2}M_3'^2\right)^{-\frac{\gamma}{\gamma-1}}\right]\right\}^{\frac{\gamma-1}{\gamma}} - 1}{\left(\frac{T_4 - T_3}{T_3}\right)} \tag{A7}$$

8. Work coefficient (ref. 2)

$$\Delta H/U_t^2 = \frac{gJc_pT_{st}\left(\frac{T_4 - T_1}{T_1}\right)}{(U_t/\sqrt{\theta})^2}$$

or, in terms of the physical constants used for this investigation,

$$\Delta H/U_t^2 = \frac{3.1455\left(\frac{T_4 - T_1}{T_1}\right)10^6}{(U_t/\sqrt{\theta})^2} \tag{A8}$$

## REFERENCES

1. Lieblein, Seymour, Lewis, George W., Jr., and Sandercock, Donald M.: Experimental Investigation of an Axial-Flow Compressor Inlet Stage Operating at Transonic Relative Inlet Mach Numbers. I - Over-All Performance of Stage with Transonic Rotor and Subsonic Stators up to Rotor Relative Inlet Mach Number of 1.1. NACA RM E52A24, 1952.

2. Schwenk, Francis C., Lieblein, Seymour, and Lewis, George W., Jr.: Experimental Investigation of an Axial-Flow Compressor Inlet Stage Operating at Transonic Relative Inlet Mach Numbers. III - Blade-Row Performance of Stage with Transonic Rotor and Subsonic Stator at Corrected Tip Speeds of 800 and 1000 Feet Per Second. NACA RM E53G17, 1953.

3. Serovy, George K., Robbins, William H., and Glaser, Frederick W.: Experimental Investigation of a 0.4 Hub-Tip Diameter Ratio Axial-Flow Compressor Inlet Stage at Transonic Inlet Relative Mach Numbers. I - Rotor Design and Over-All Performance at Tip Speeds from 60 to 100 Percent of Design. NACA RM E53I11, 1953.

4. Savage, Melvyn, Erwin, John R., and Whitley, Robert P.: Investigation of an Axial-Flow Compressor Rotor Having NACA High-Speed Blade Sections ($A_2I_{8b}$ Series) at Mean Radius Relative Inlet Mach Numbers up to 1.13. NACA RM L53G02, 1953.

5. Andrews, S. J.: Tests Related to the Effect of Profile Shape and Camber Line on Compressor Cascade Performance. Rep. No. R.60, British N.G.T.E., Oct. 1949.

6. Lieblein, Seymour, Schwenk, Francis C., and Broderick, Robert L.: Diffusion Factor for Estimating Losses and Limiting Blade Loading in Axial-Flow-Compressor Blade Elements. NACA RM E53D01, 1953.

7. Schulze, Wallace M., Erwin, John R., and Ashby, George C., Jr.: NACA 65-Series Compressor Rotor Performance with Varying Annulus-Area Ratio, Solidity, Blade Angle, and Reynolds Number and Comparison with Cascade Results. NACA RM L52L17, 1953.

8. Jeffs, R. A., Hounsell, A. F., and Adams, R. G.: Further Performance Data for Aerofoils Having C.1, C.2, or C.4 Base Profiles on Circular Arc Camber Lines. Memo. No. M.139, British N.G.T.E., 1951.

9. Carter, A. D. S.: The Low Speed Performance of Related Aerofoils in Cascade. Rep. No. R.55, British N.G.T.E., Sept. 1949.

TABLE I. - ROTOR-BLADE-ELEMENT GEOMETRY

| Radial position | Radius, in. | | Solidity, $\sigma$ | Blade inlet angle, $\gamma_3^o$, deg | Blade outlet angle, $\gamma_4^o$, deg |
|---|---|---|---|---|---|
| | Inlet, $r_3$ | Outlet, $r_4$ | | | |
| 4 | 7.969 | 8.098 | 1.32 | 53.5 | 30.9 |
| 5 | 7.257 | 7.515 | 1.41 | 51.2 | 26.9 |
| 6 | 6.546 | 6.933 | 1.525 | 48.5 | 21.8 |
| 7 | 5.834 | 6.350 | 1.65 | 45.7 | 15.4 |
| 8 | 5.123 | 5.768 | 1.80 | 42.6 | 7.8 |

TABLE II. - STATOR-BLADE-ELEMENT GEOMETRY

| Radial position | Radius, in. | | Solidity, $\sigma$ | Blade inlet angle, $\gamma_4^o$, deg | Blade outlet angle, $\gamma_5^o$, deg |
|---|---|---|---|---|---|
| | Inlet, $r_4$ | Outlet, $r_5$ | | | |
| 3 | 8.098 | 8.225 | 1.18 | 36.0 | [a]-16.0 |
| 5 | 7.515 | 7.770 | 1.29 | ↓ | ↓ |
| 6 | 6.933 | 7.315 | 1.39 | ↓ | ↓ |
| 7 | 6.350 | 6.860 | 1.49 | ↓ | ↓ |
| 9 | 5.768 | 6.405 | 1.59 | ↓ | ↓ |

[a]Negative angles indicate angles past axial direction.

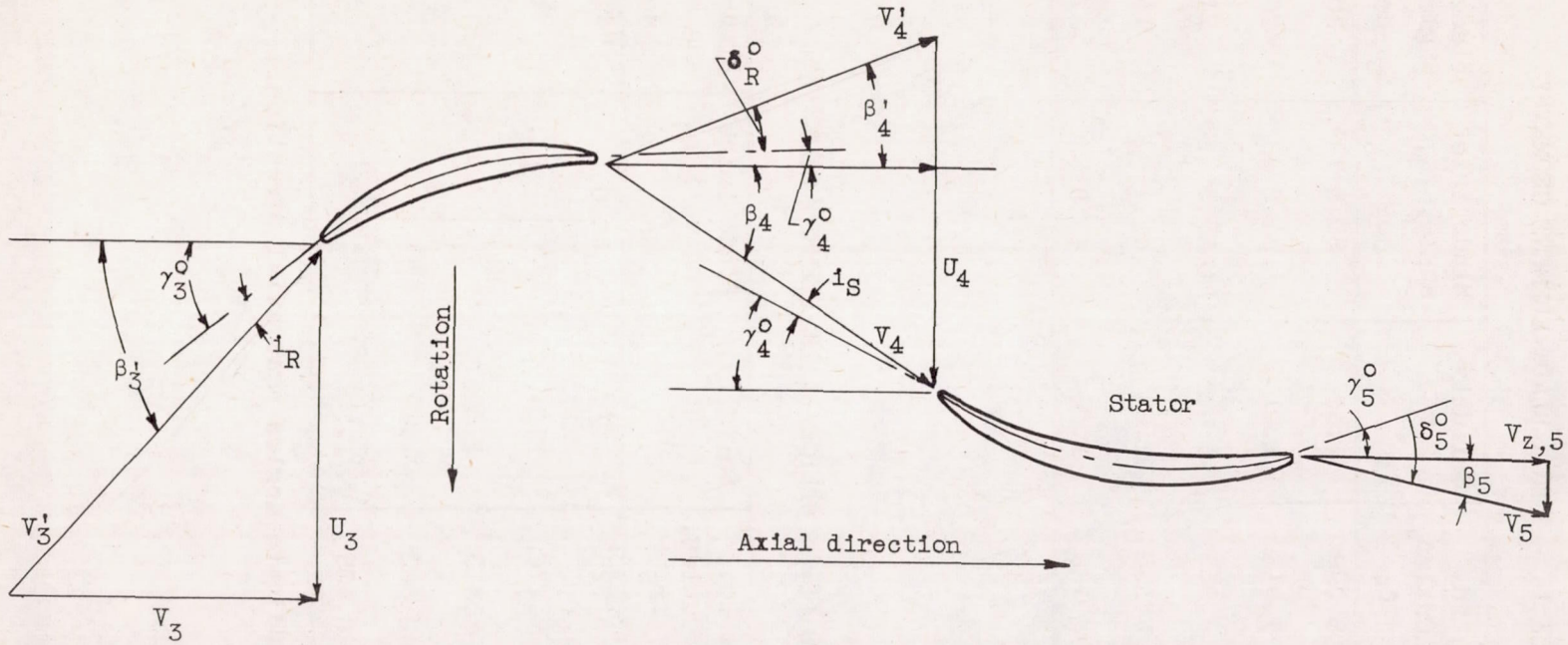


Figure 1. - Velocity-diagram notation for blade element.

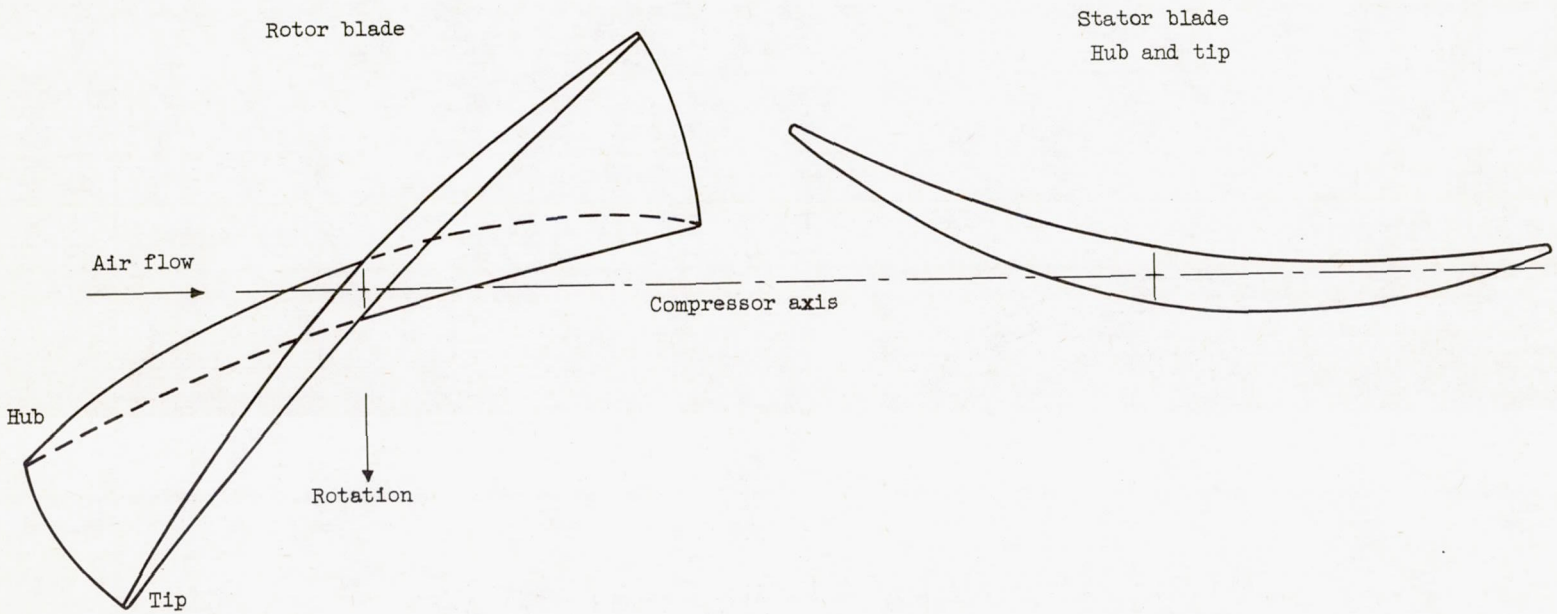


Figure 2. - Rotor- and stator-blade profiles at hub and tip.

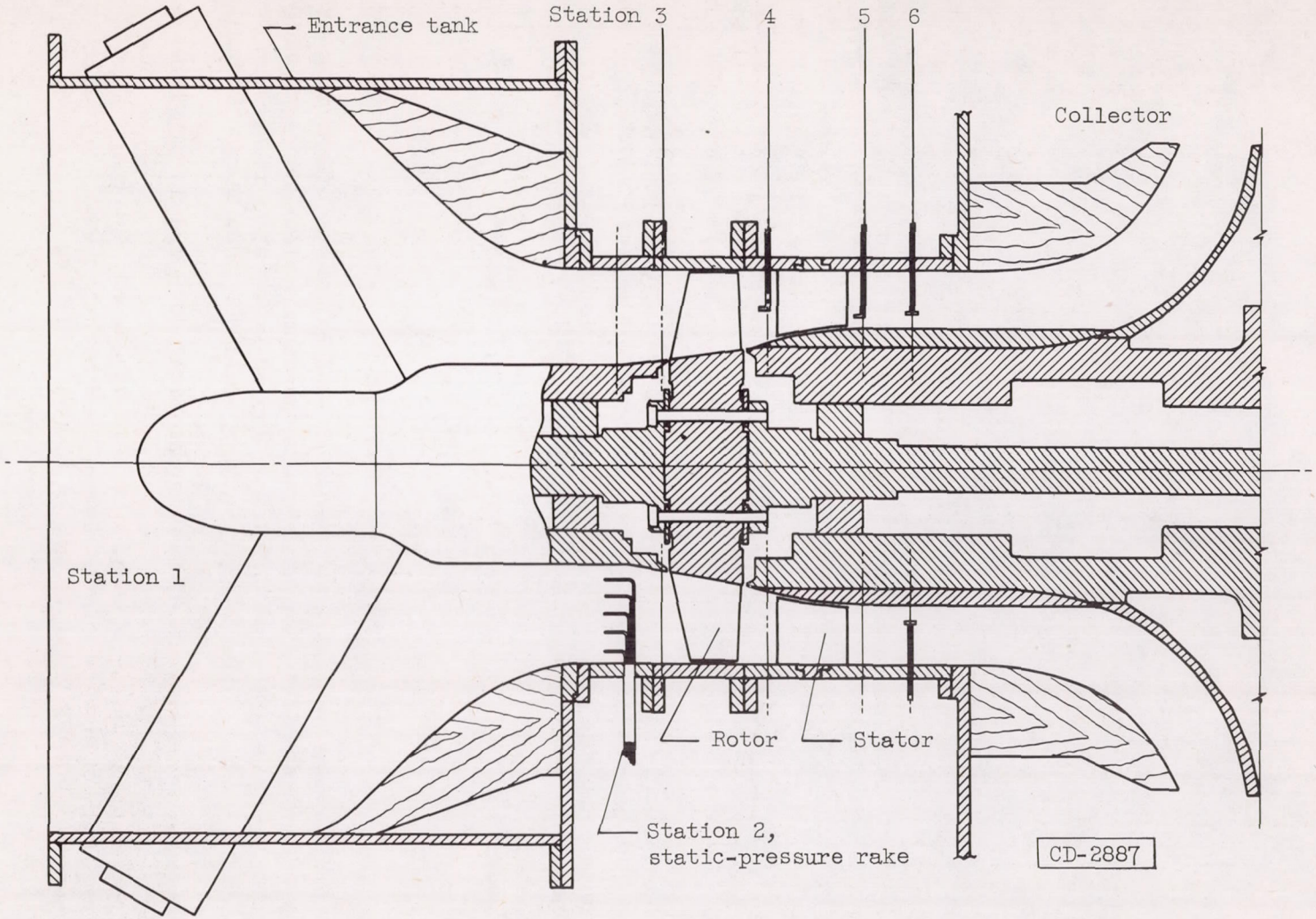


Figure 3. - Schematic diagram of variable-component transonic-compressor test rig.

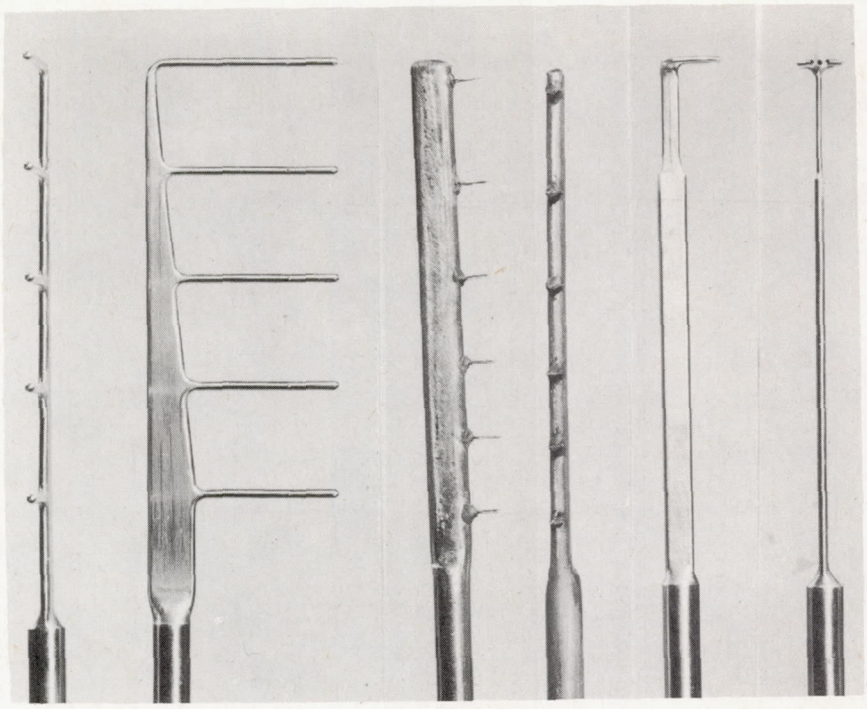

(a) Inlet static-pressure rake.

(b) Thermocouple rake.

(c) Claw and total-pressure survey probe.

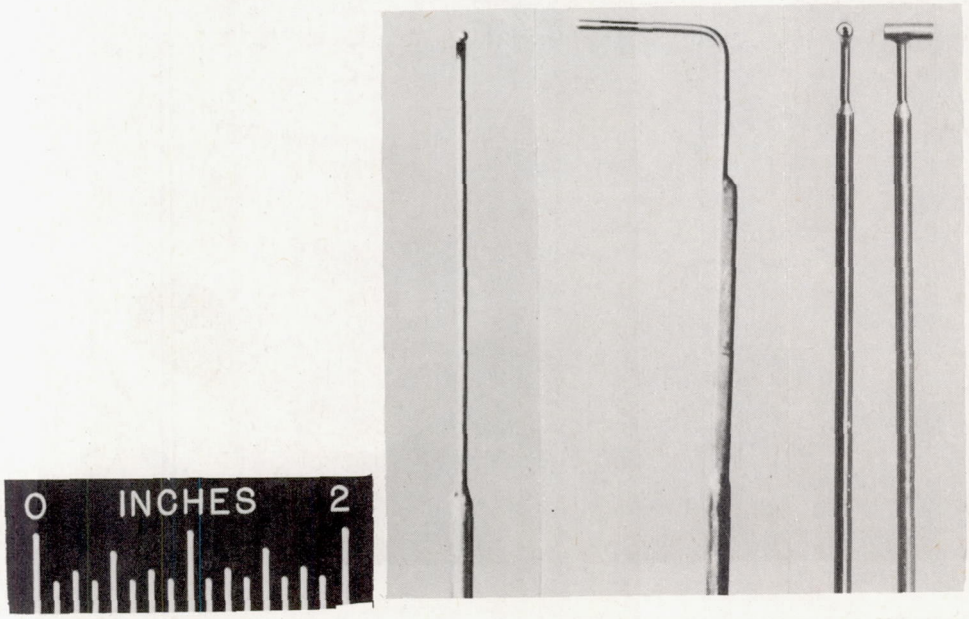


C-35272

(d) Static-pressure survey probe.

(e) Kiel probe.

Figure 4. - Instrumentation used for investigation of transonic inlet stage.

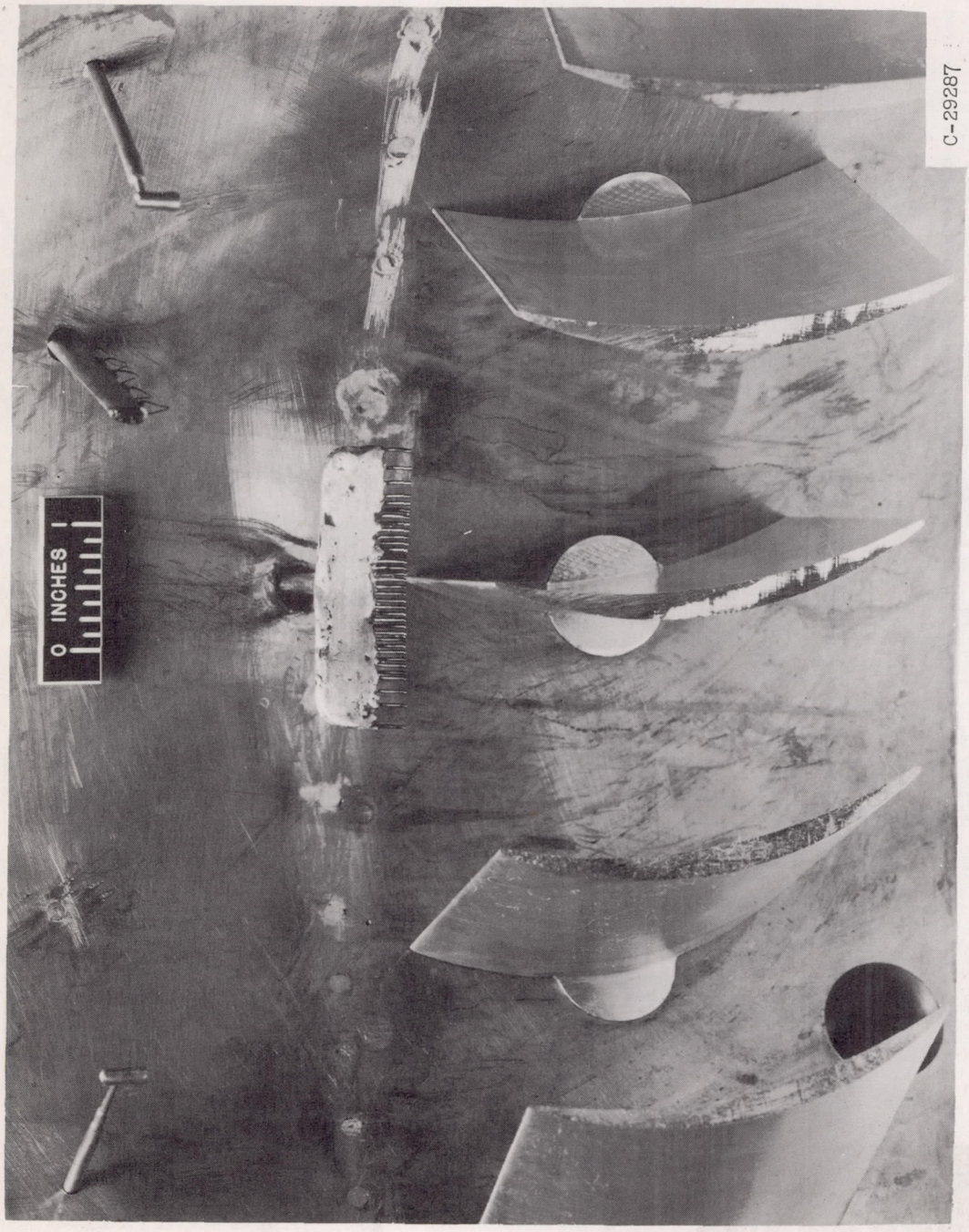


Figure 5. - Total-pressure rake for measuring loss in stators.

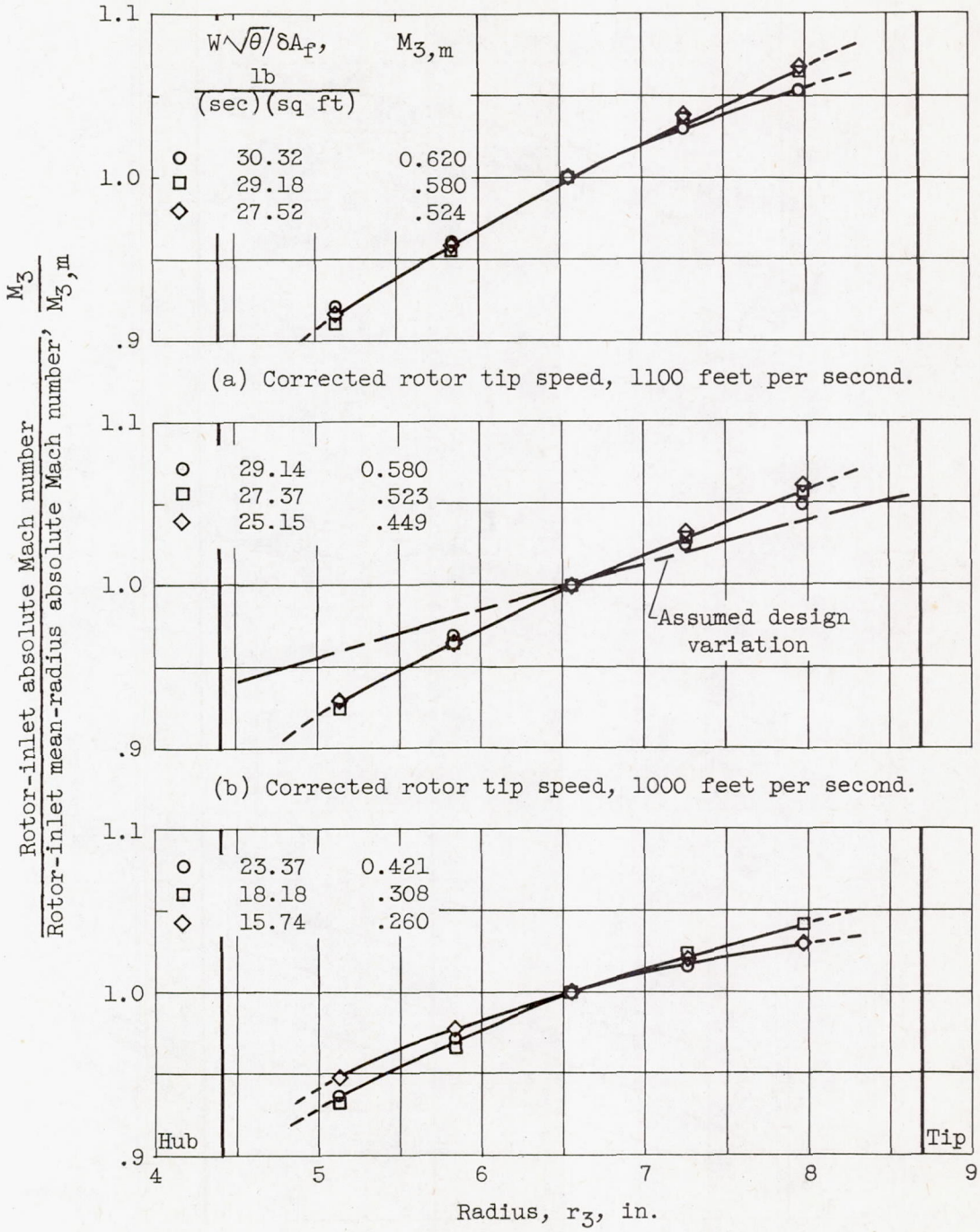


(a) Corrected rotor tip speed, 1100 feet per second.

(b) Corrected rotor tip speed, 1000 feet per second.

(c) Corrected rotor tip speed, 600 feet per second.

Figure 6. - Radial variation of rotor-inlet absolute Mach number (station 3).

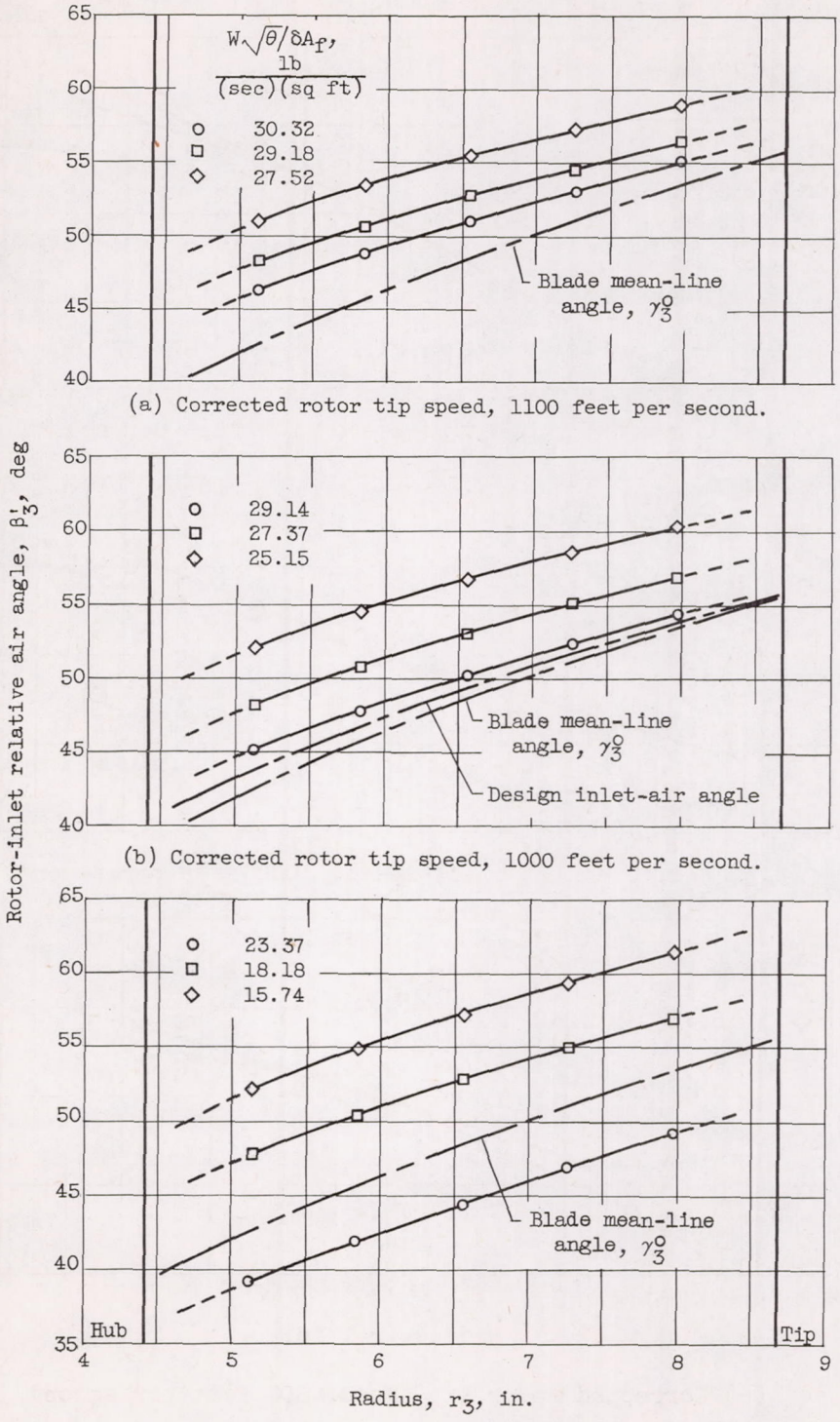


(a) Corrected rotor tip speed, 1100 feet per second.

(b) Corrected rotor tip speed, 1000 feet per second.

(c) Corrected rotor tip speed, 600 feet per second.

Figure 7. - Radial variation of rotor-inlet relative angles (station 3).

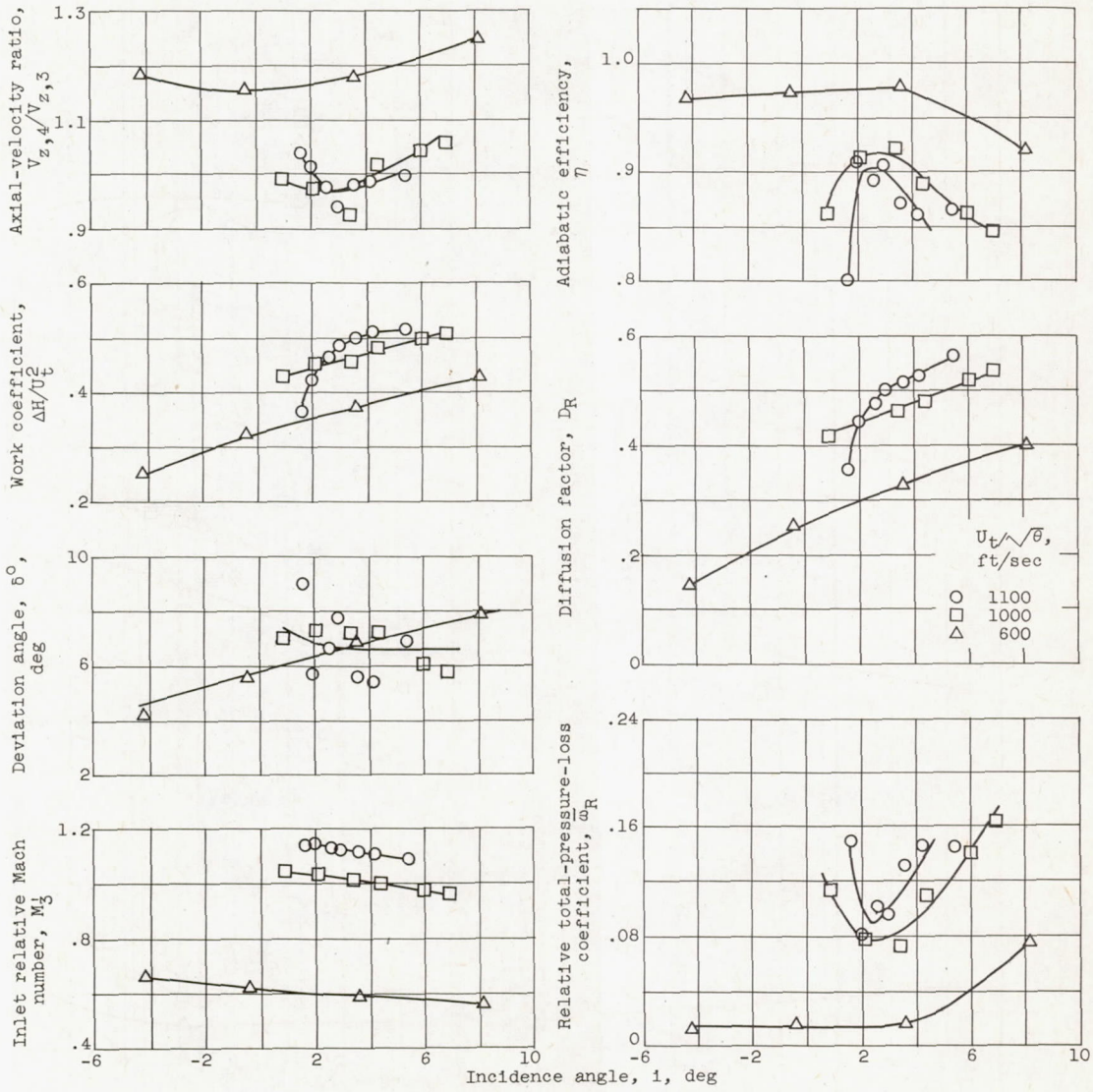


(a) Position 4; radius, 8.098 inches (near tip).

Figure 8. - Rotor-blade-element characteristics.

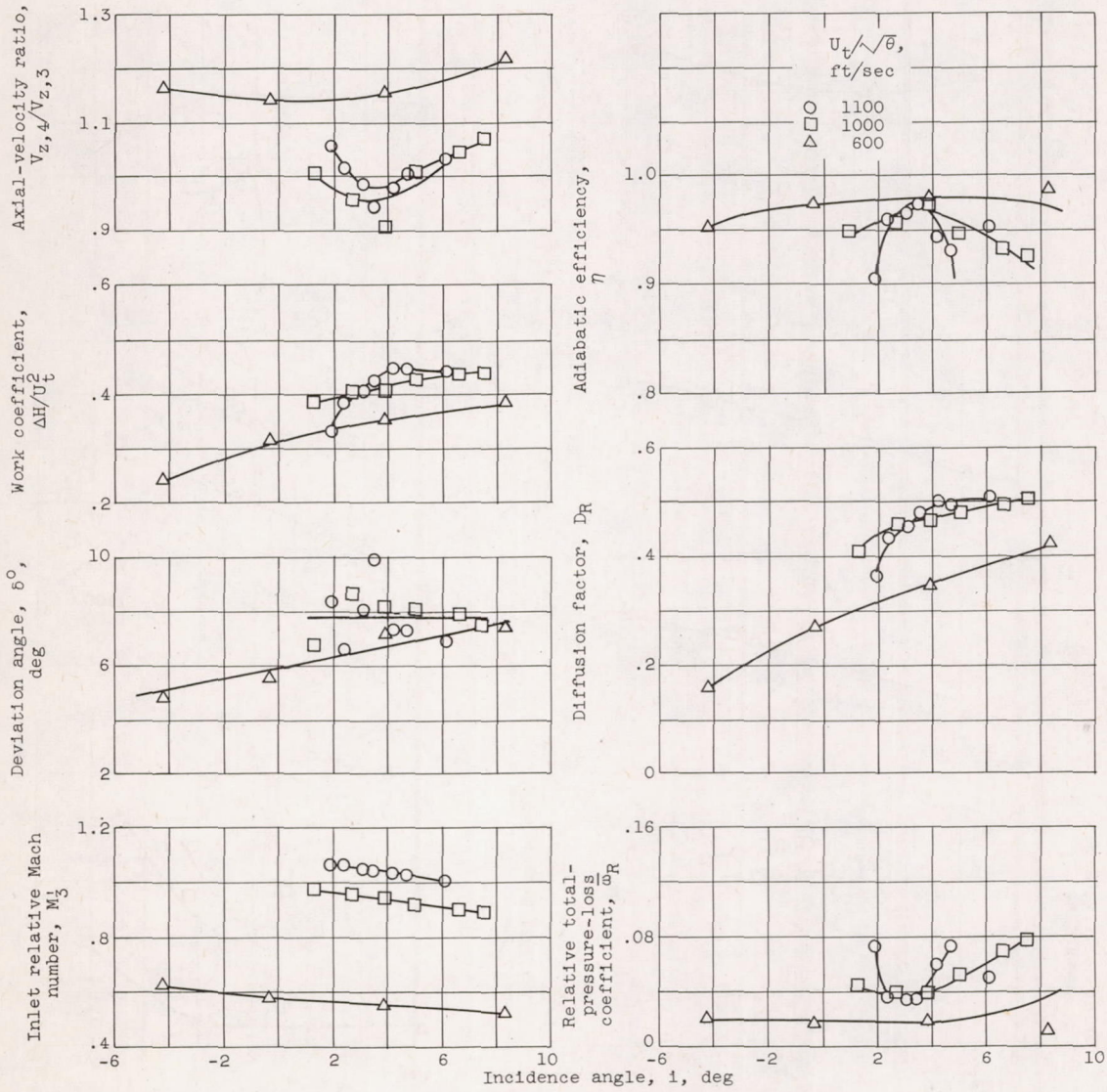


(b) Position 5; radius, 7.515 inches.

Figure 8. - Continued. Rotor-blade-element characteristics.

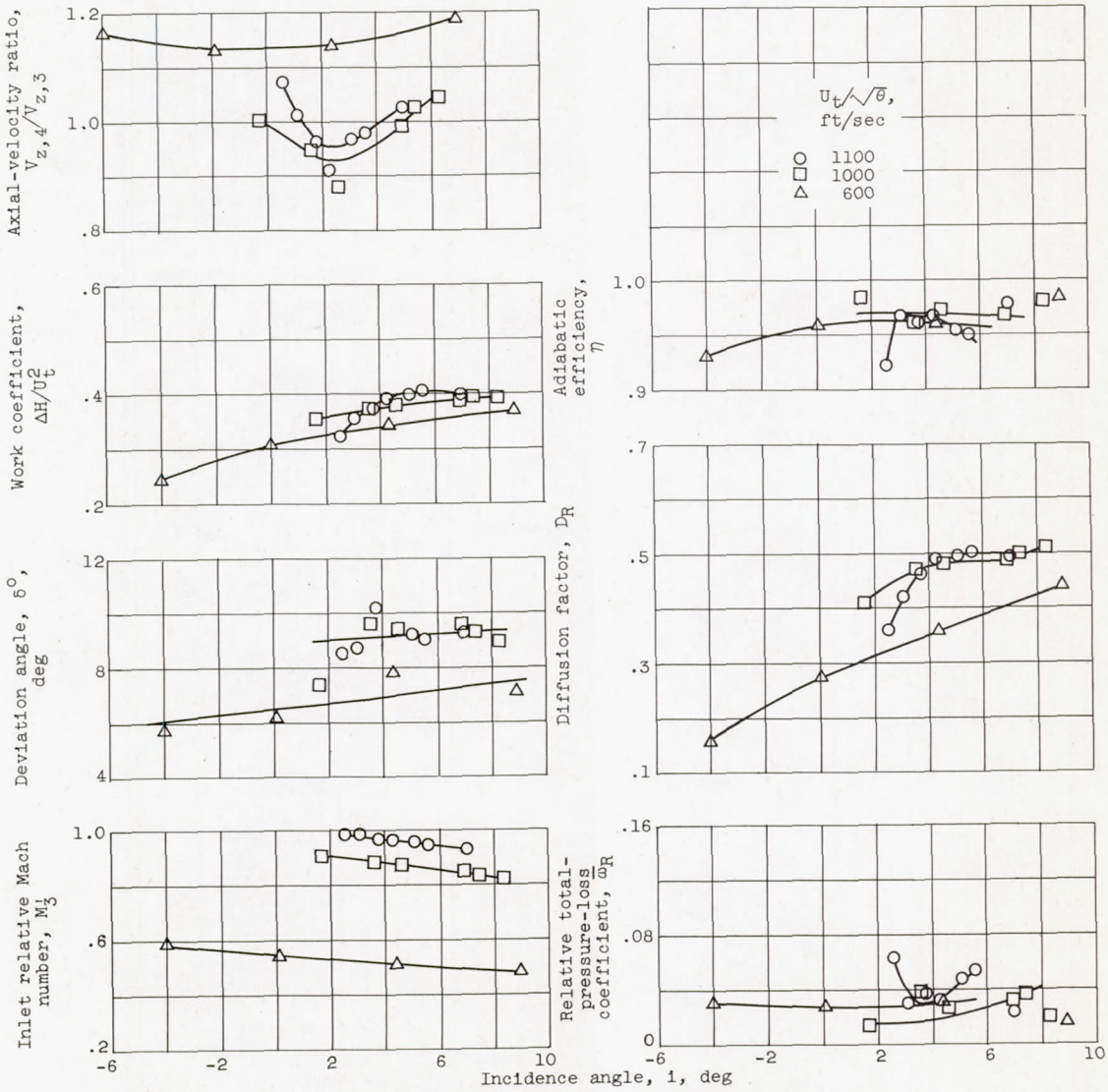


(c) Position 6; radius, 6.933 inches (mean radius).

Figure 8. - Continued. Rotor-blade-element characteristics.

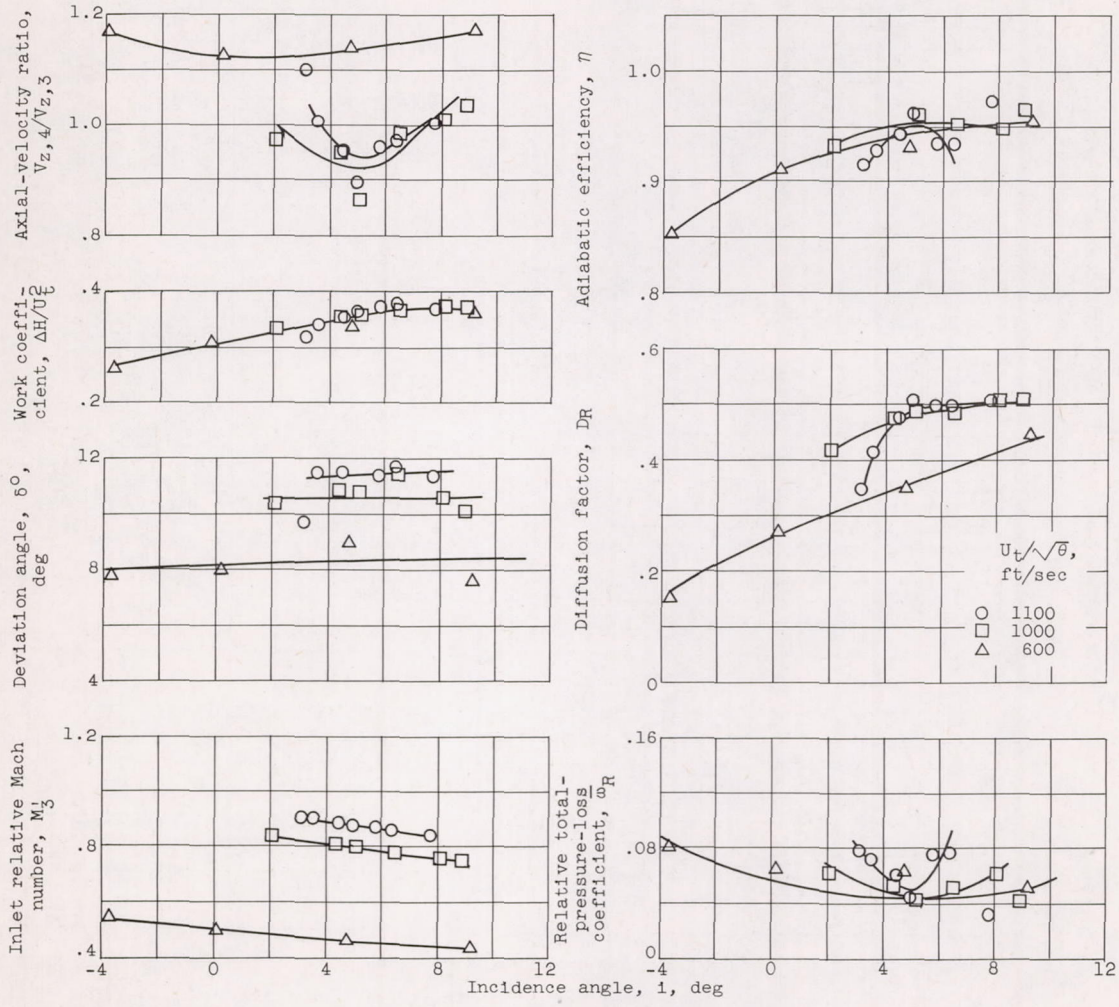


(d) Position 7; radius, 6.350 inches.

Figure 8. - Continued. Rotor-blade-element characteristics.

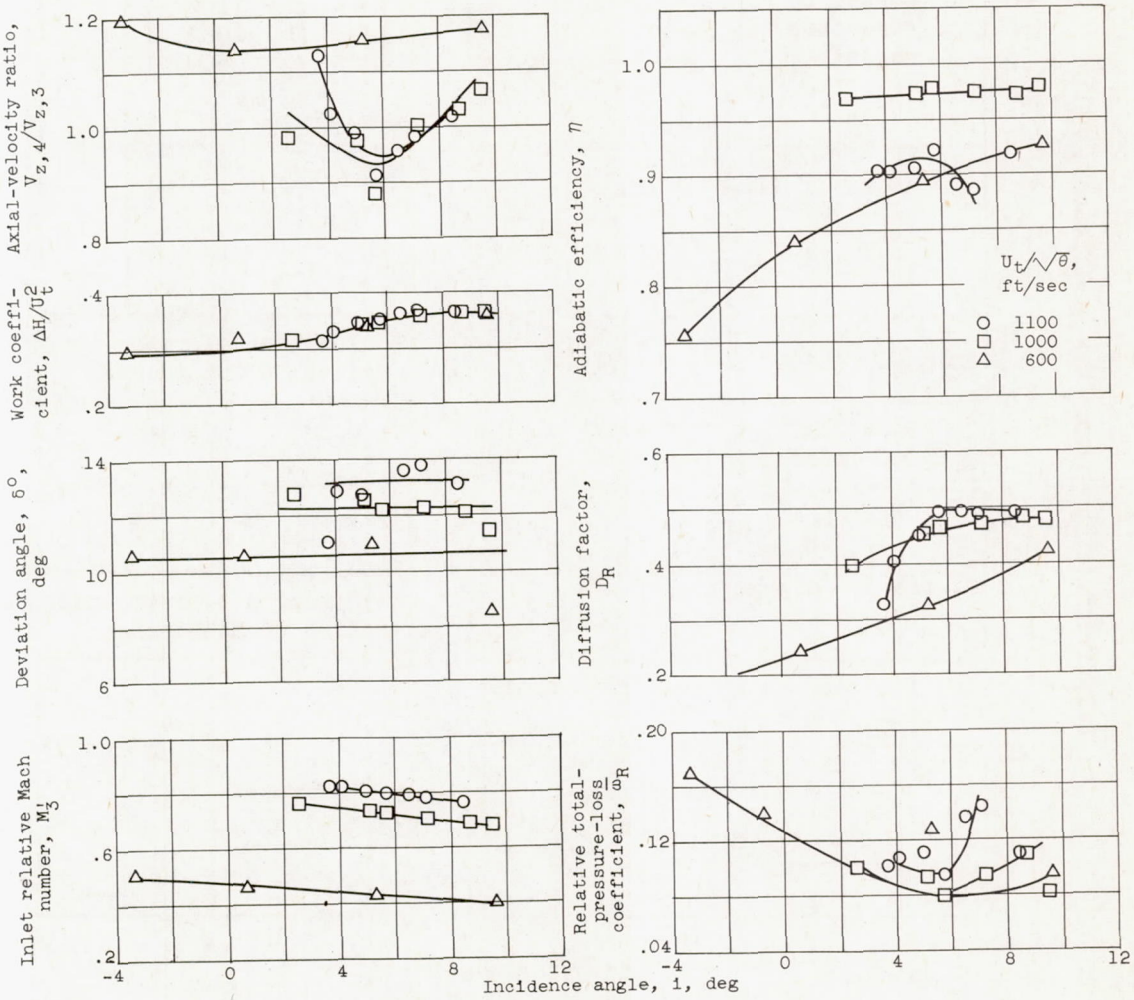


(e) Position 8; radius, 5.768 inches (near hub).

Figure 8. - Concluded. Rotor-blade-element characteristics.

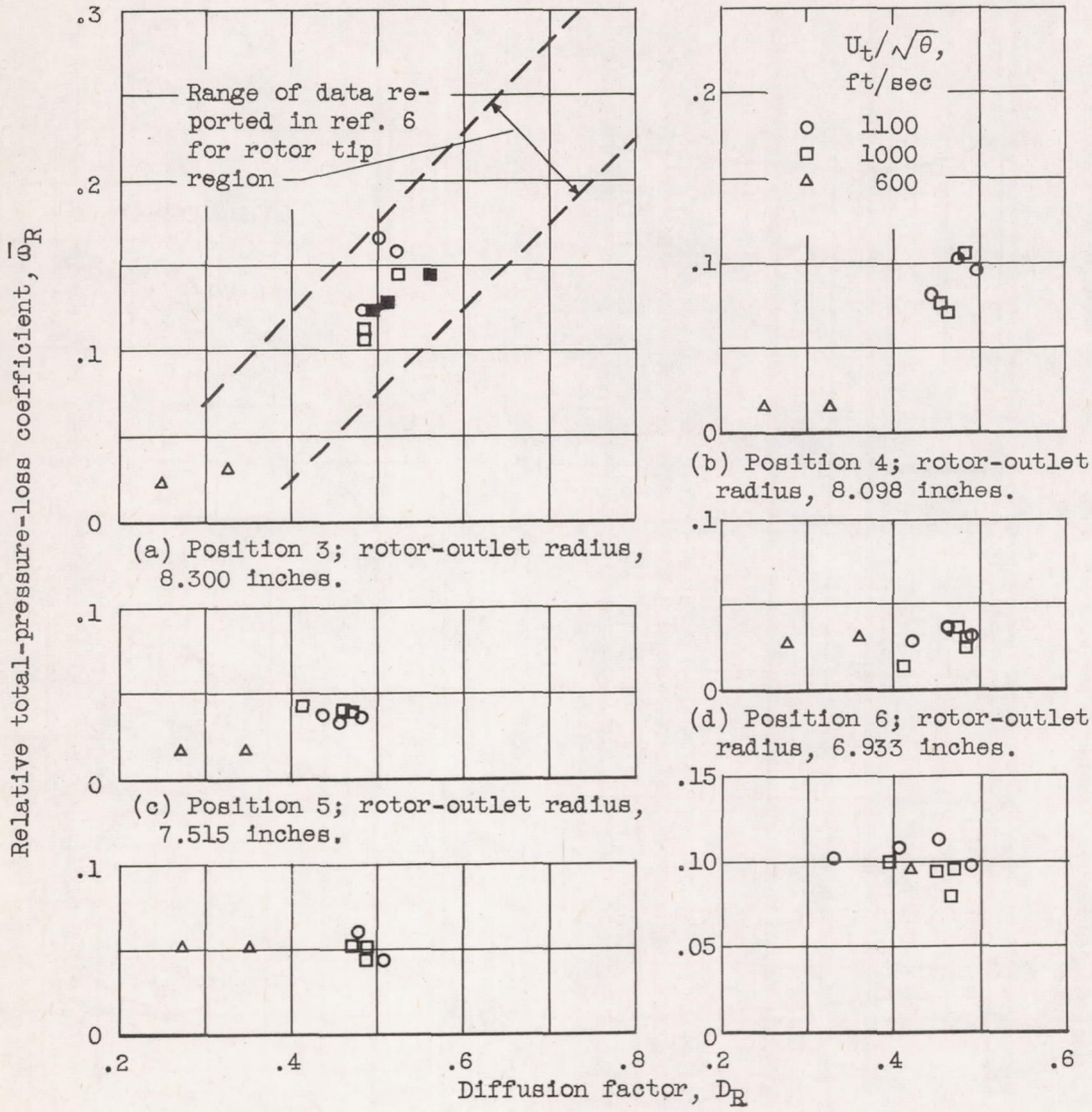


(a) Position 3; rotor-outlet radius, 8.300 inches.

(b) Position 4; rotor-outlet radius, 8.098 inches.

(c) Position 5; rotor-outlet radius, 7.515 inches.

(d) Position 6; rotor-outlet radius, 6.933 inches.

(e) Position 7; rotor-outlet radius, 6.350 inches.

(f) Position 8; rotor-outlet radius, 5.768 inches.

Figure 9. - Variation of rotor-blade-element losses with diffusion factor in low-loss range of incidence angle. (Solid symbols are data obtained for same rotor reported in ref. 2.)

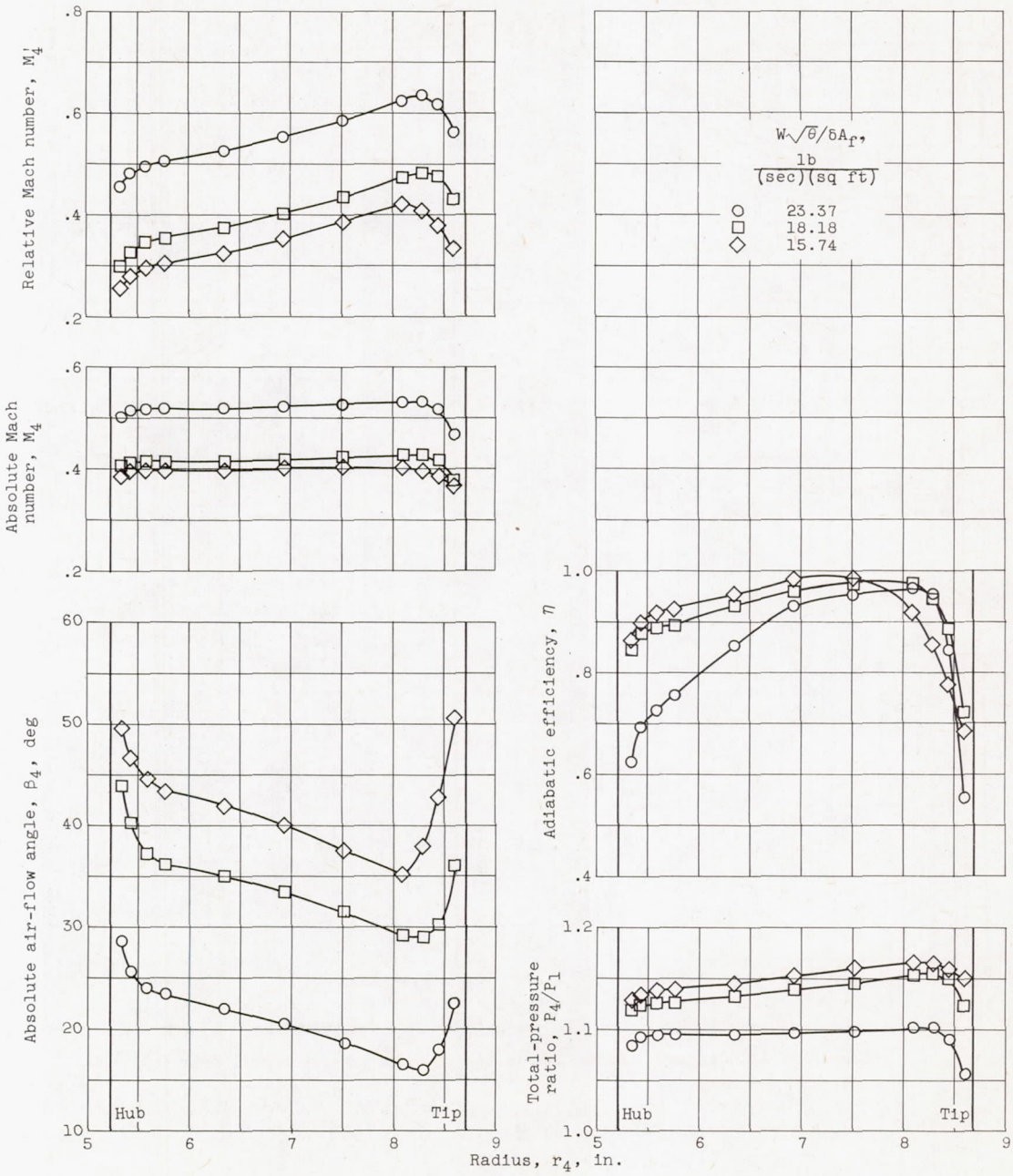


(a) Corrected rotor tip speed, 600 feet per second.

Figure 10. - Radial variation of rotor-outlet conditions.

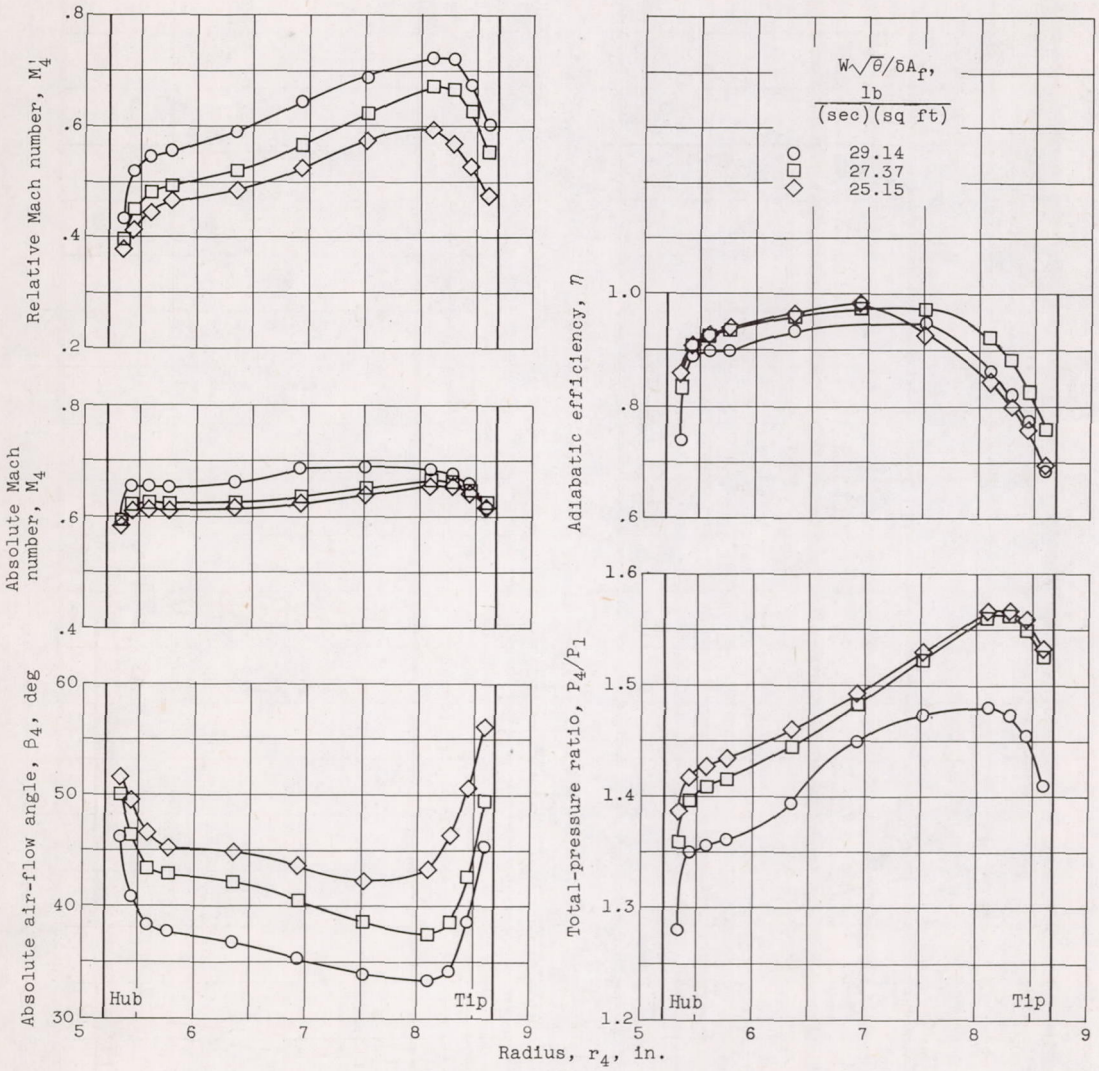


(b) Corrected rotor tip speed, 1000 feet per second.

Figure 10. - Continued. Radial variation of rotor-outlet conditions.

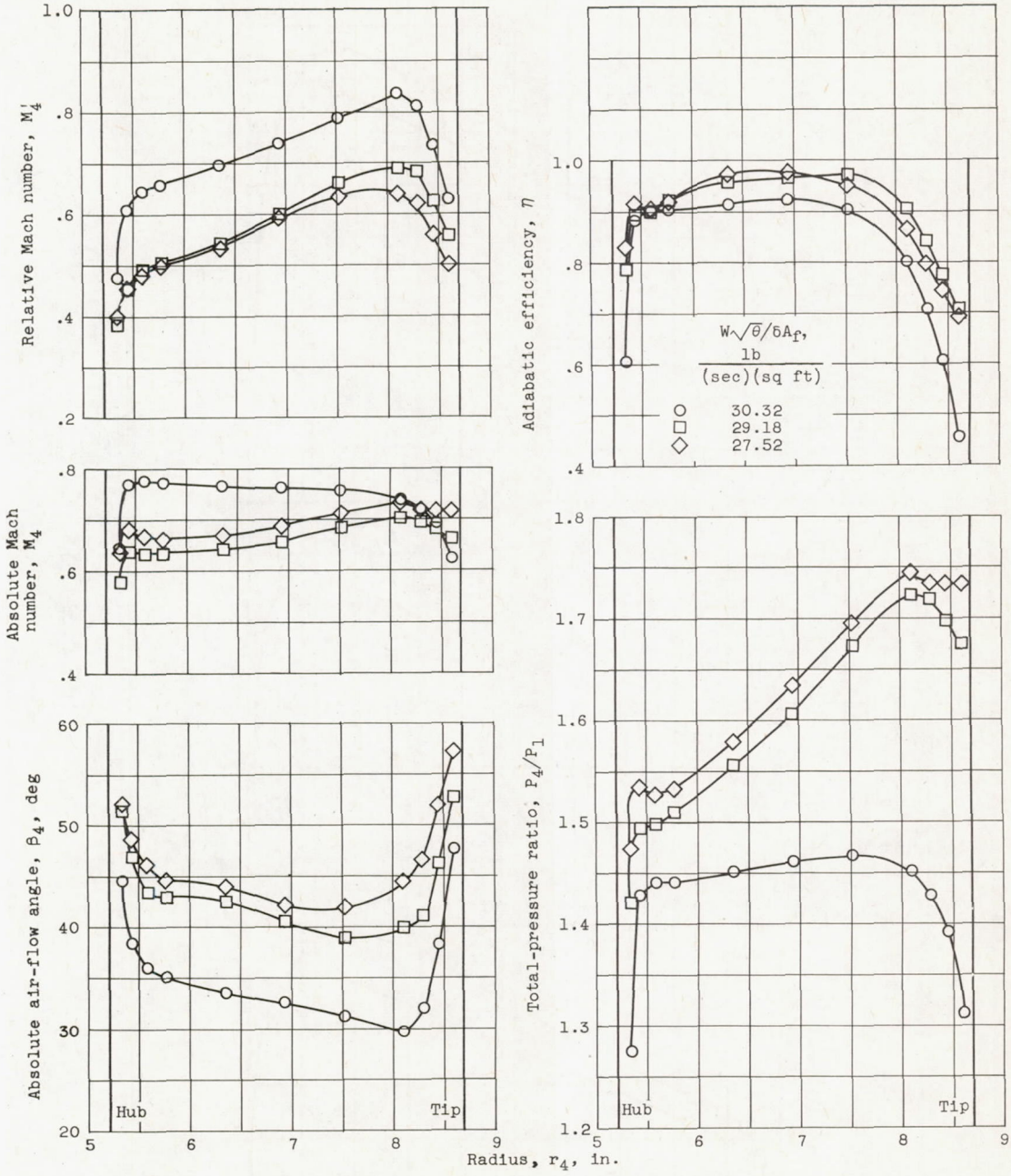


(c) Corrected rotor tip speed, 1100 feet per second.

Figure 10. - Concluded. Radial variation of rotor-outlet conditions.

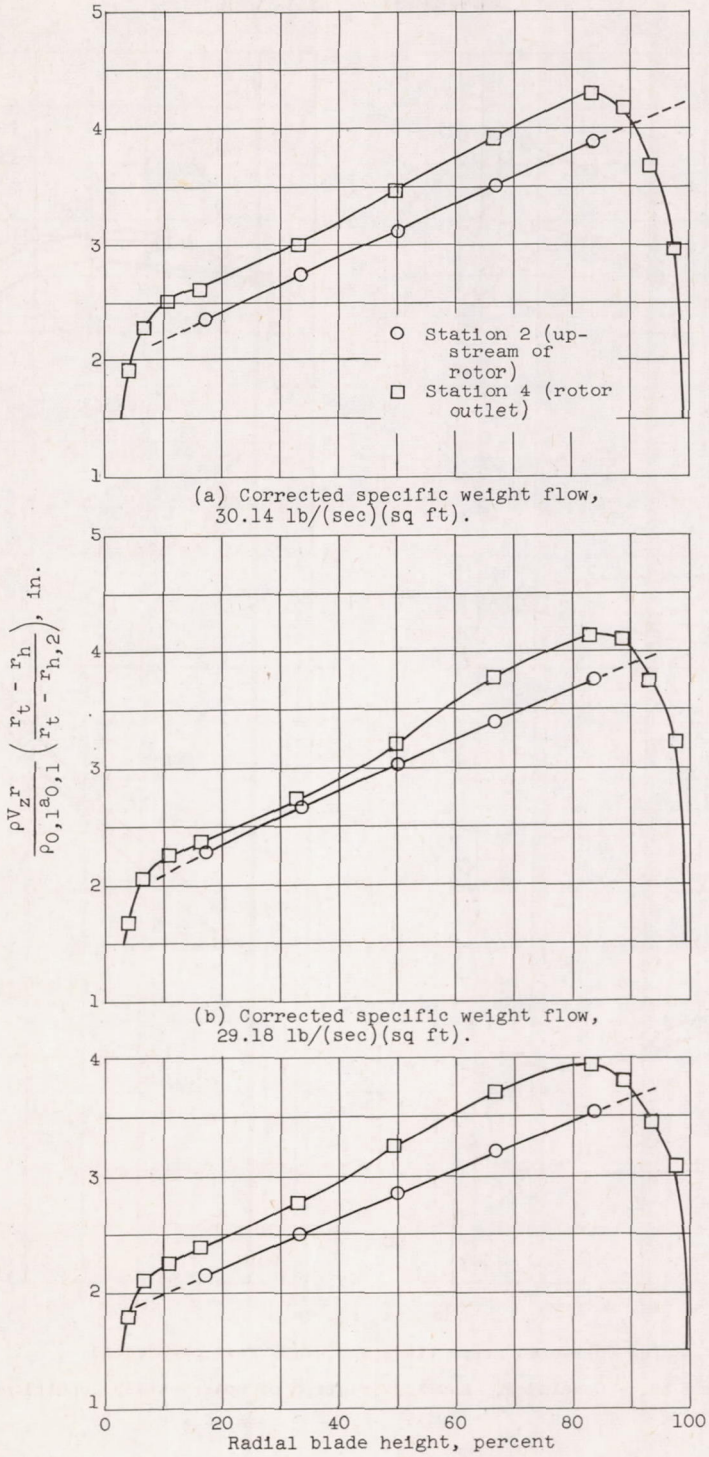


(a) Corrected specific weight flow, 30.14 lb/(sec)(sq ft).

(b) Corrected specific weight flow, 29.18 lb/(sec)(sq ft).

(c) Corrected specific weight flow, 27.52 lb/(sec)(sq ft).

Figure 11. - Radial distribution of weight flow at corrected rotor tip speed of 1100 feet per second.

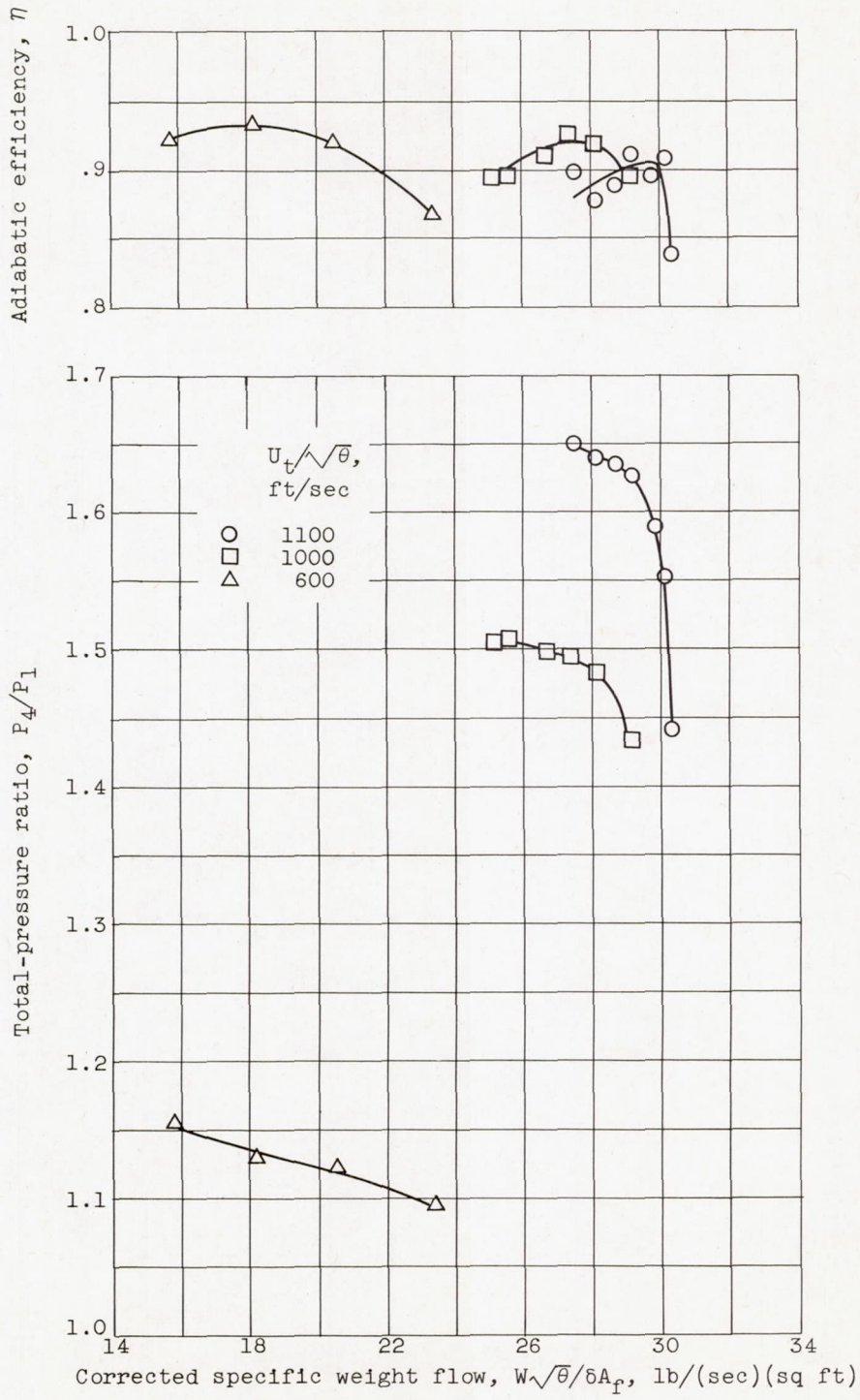


Figure 12. - Mass-averaged rotor-performance characteristics.

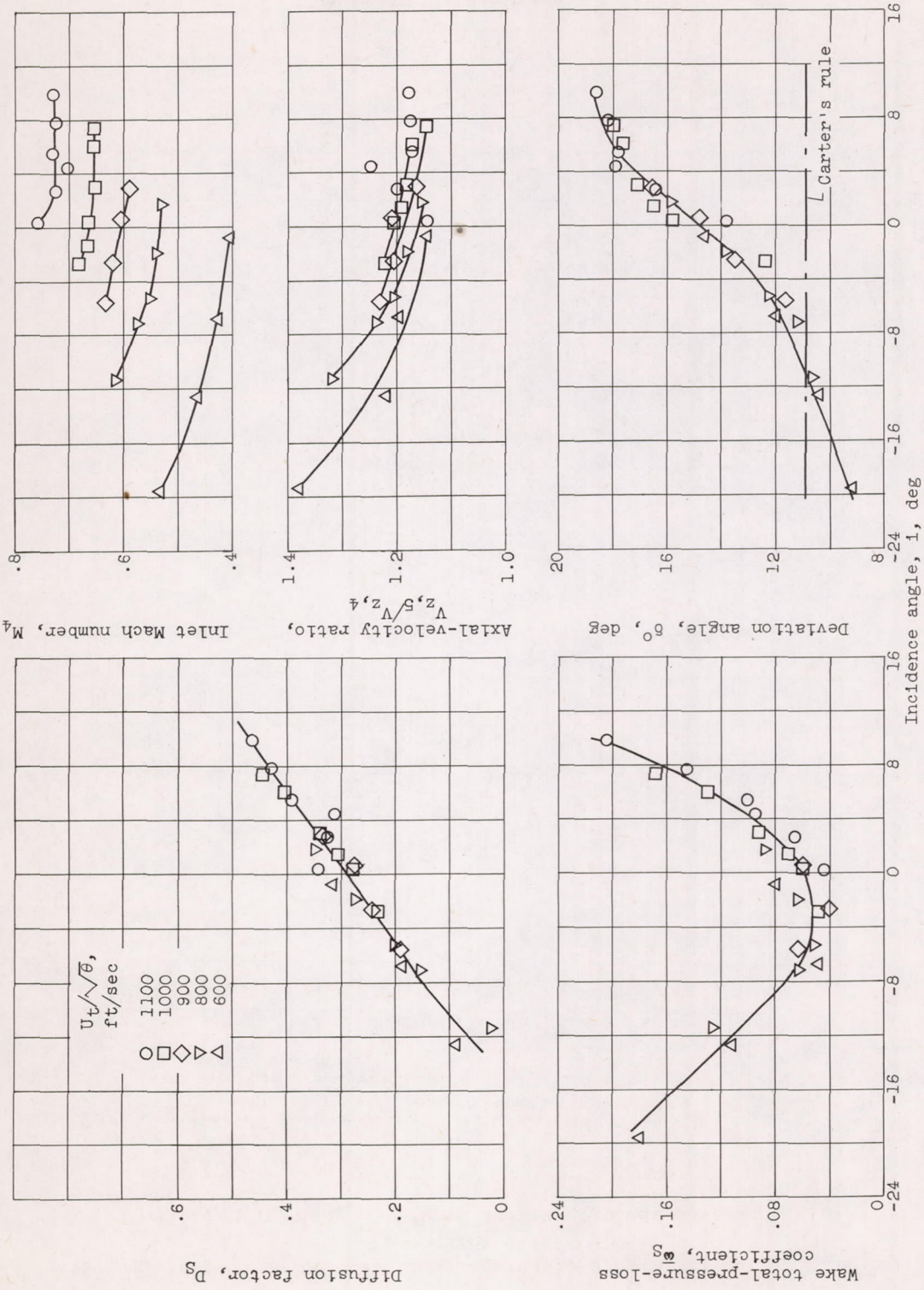


(a) Position 3; radius, 8.225 inches (near tip).

Figure 13. - Stator-blade-element characteristics.

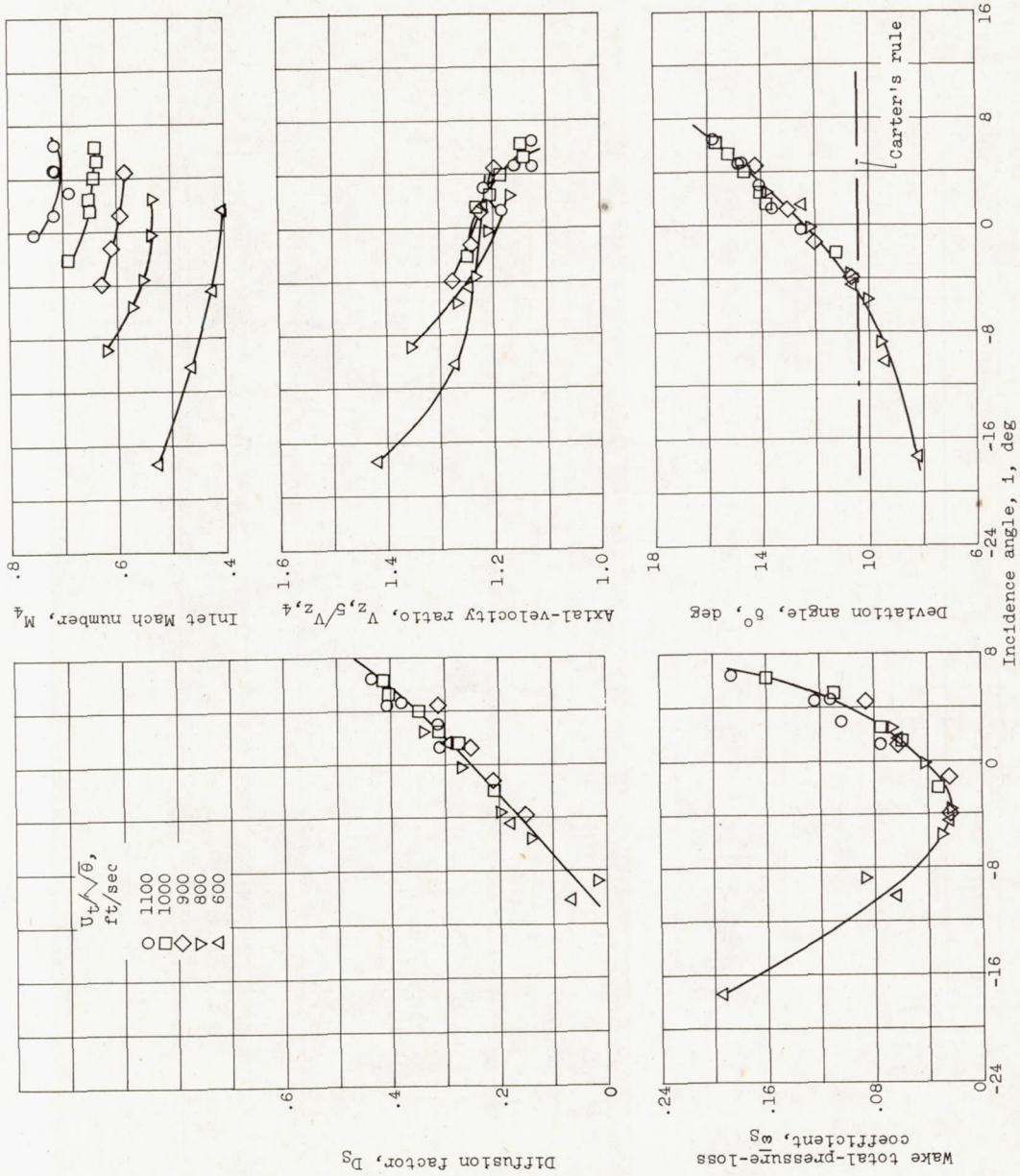


(b) Position 5; radius, 7.770 inches.

Figure 13. - Continued. Stator-blade-element characteristics.

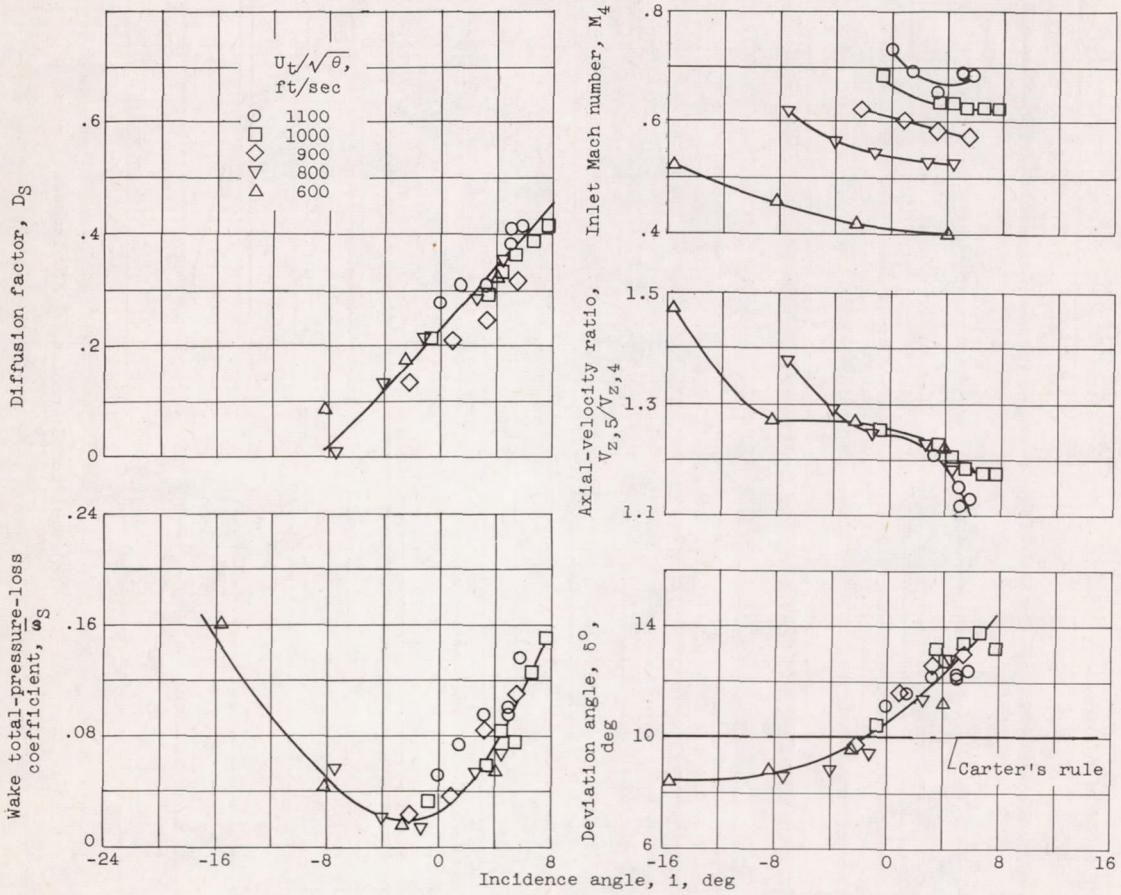


(c) Position 6; radius, 7.315 inches (mean radius).

Figure 13. - Continued. Stator-blade-element characteristics.

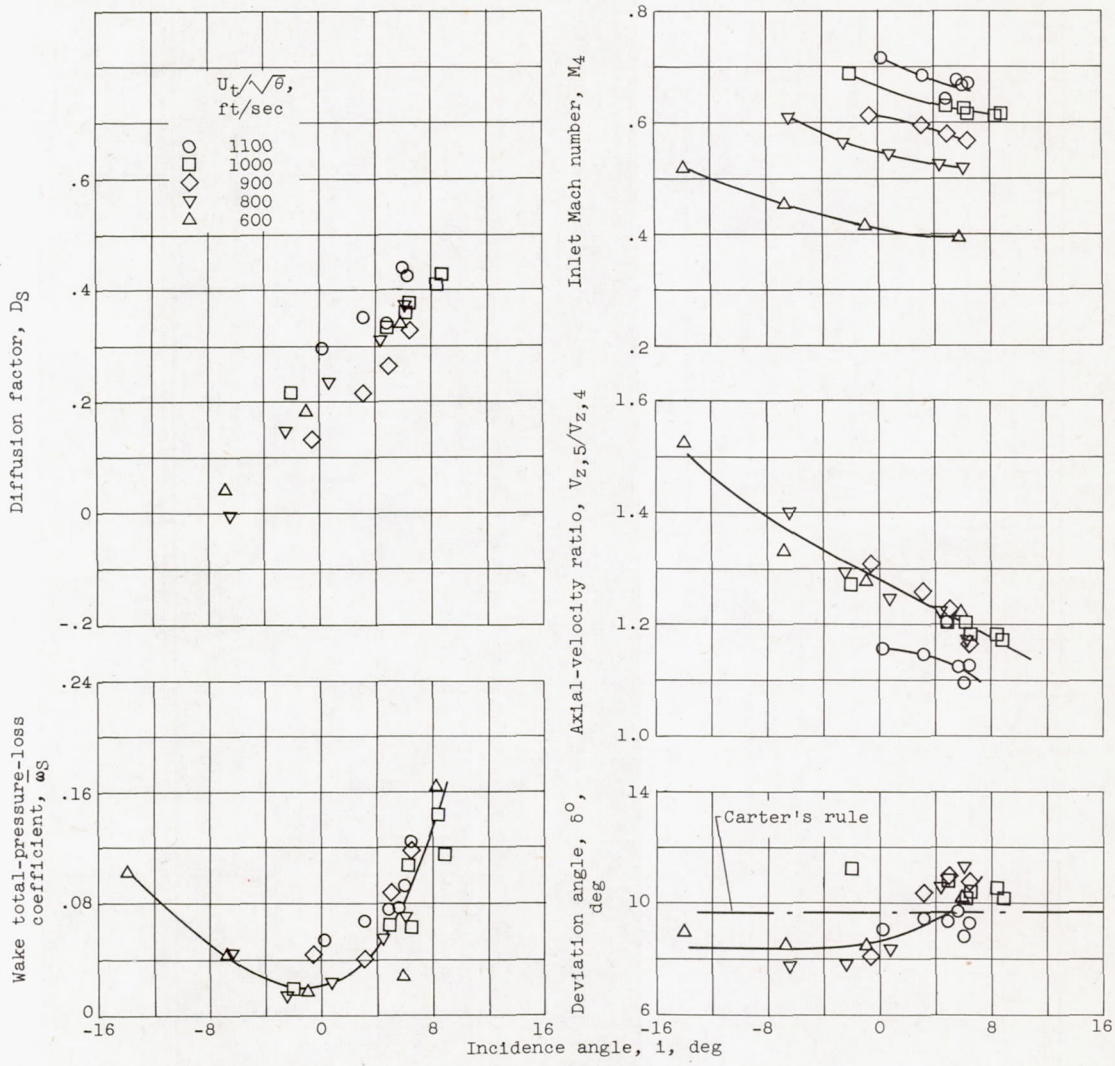


(d) Position 7; radius, 6.860 inches.

Figure 13. - Continued. Stator-blade-element characteristics.

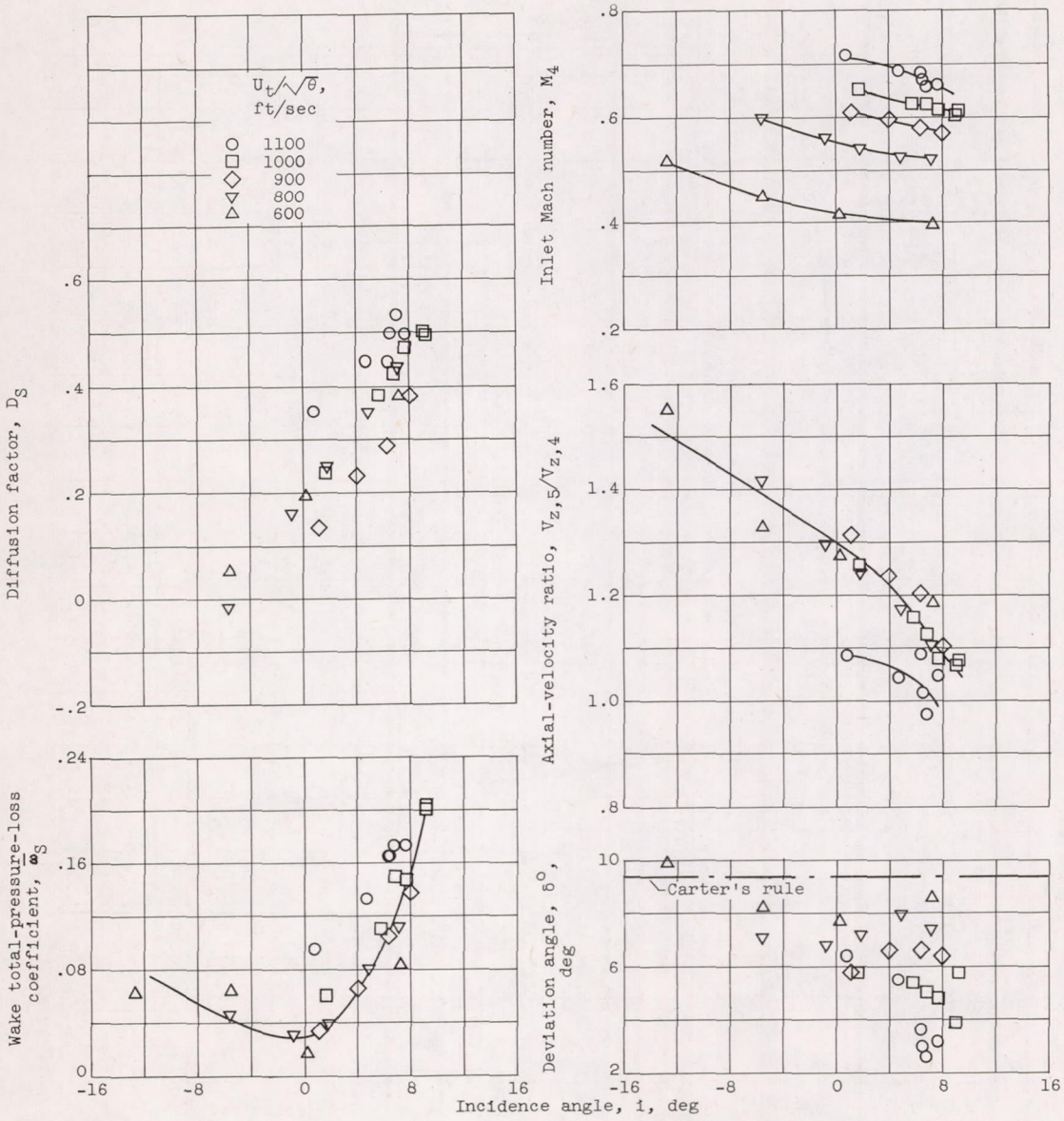


(e) Position 9; radius, 6.405 inches (near hub).

Figure 13. - Concluded. Stator-blade-element characteristics.

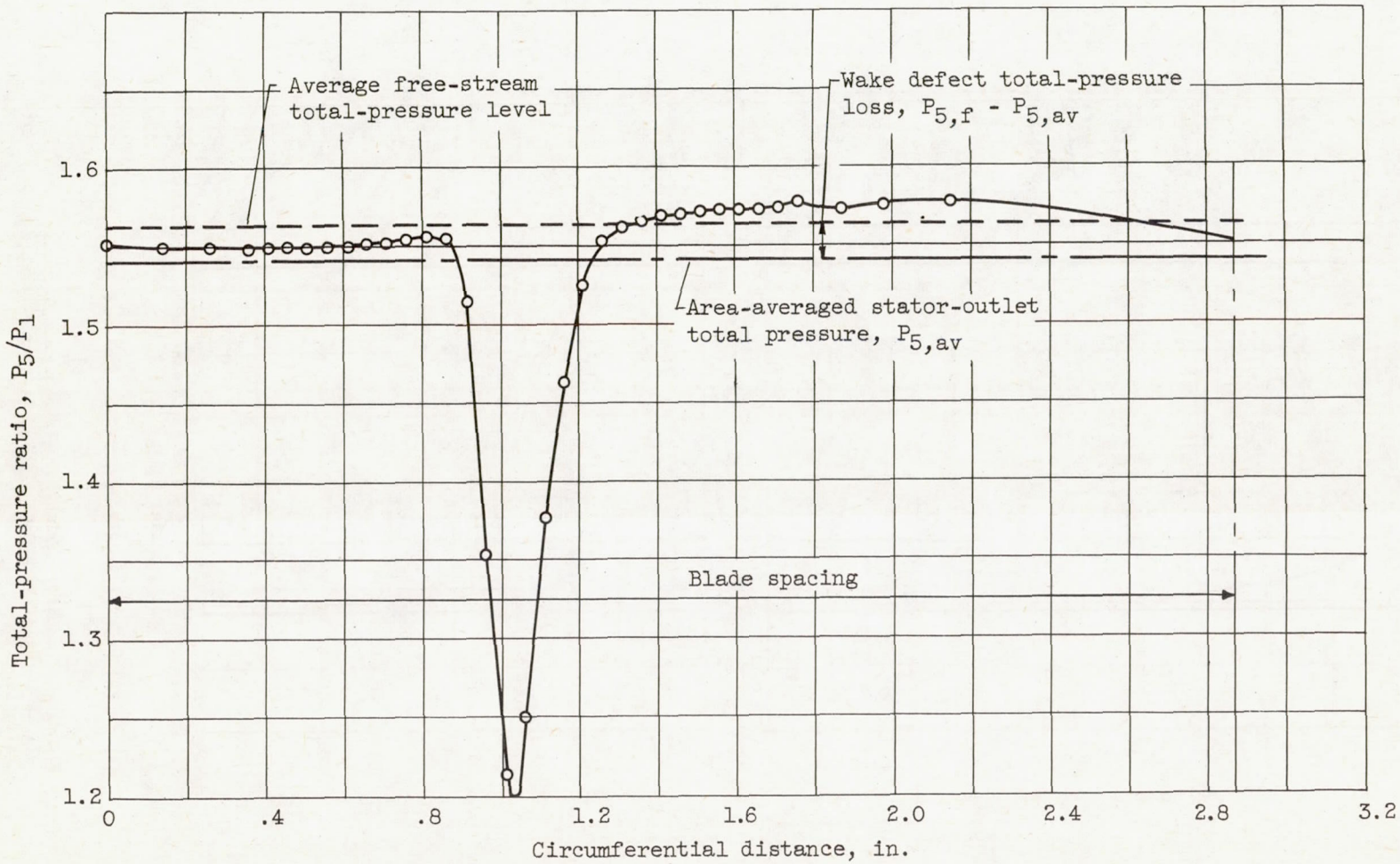


Figure 14. - Circumferential variation of total-pressure ratio measured downstream of stators (station 5, near tip).

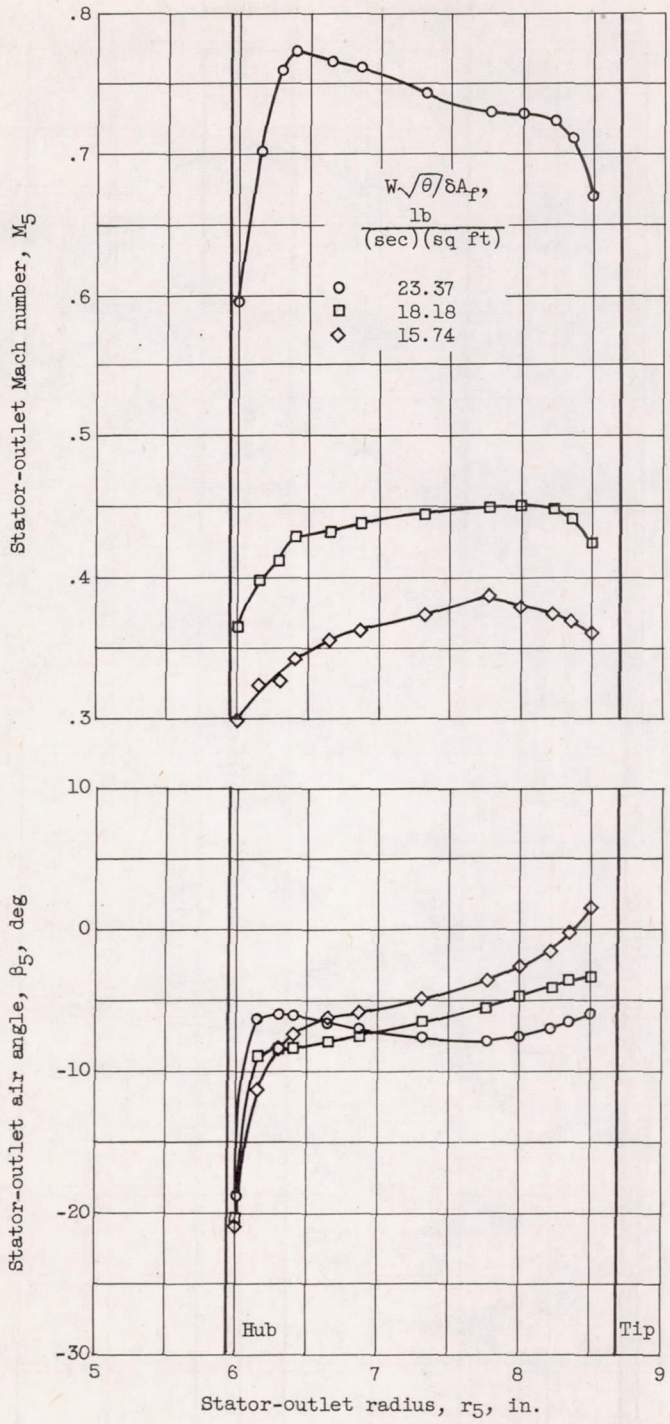


(a) Corrected rotor tip speed, 600 feet per second.

Figure 15. - Radial variation of stator-outlet conditions. (Negative angles signify turning past axial direction.)

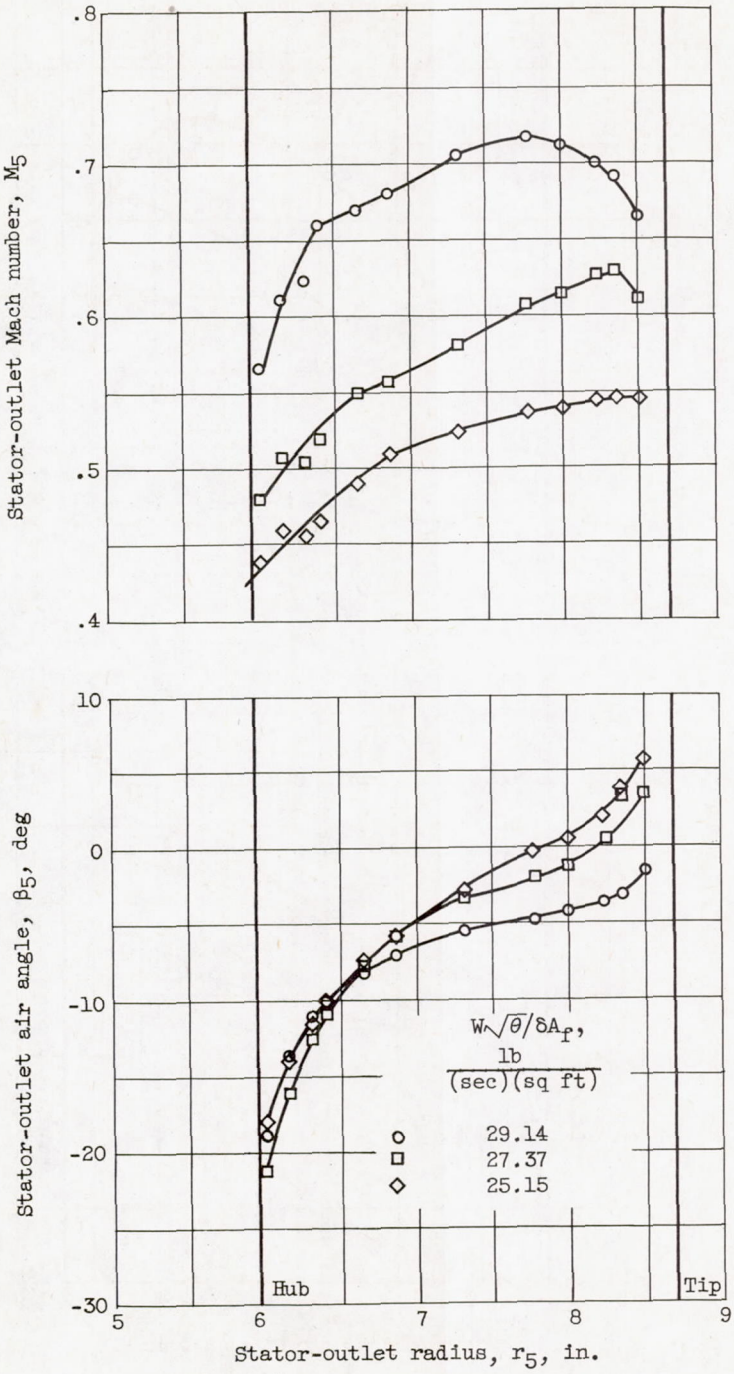


(b) Corrected rotor tip speed, 1000 feet per second.

Figure 15. - Continued. Radial variation of stator-outlet conditions. (Negative angles signify turning past axial direction.)

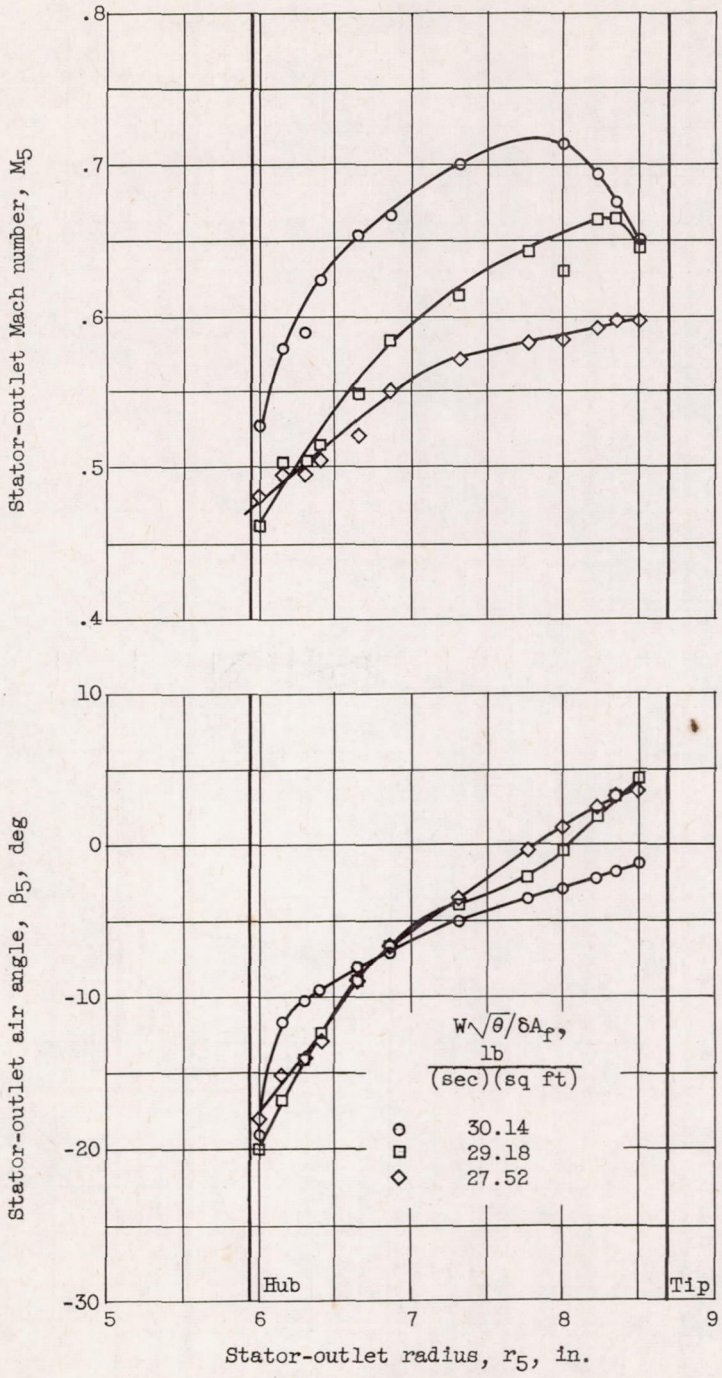


(c) Corrected rotor tip speed, 1100 feet per second.

Figure 15. - Concluded. Radial variation of stator-outlet conditions. (Negative angles signify turning past axial direction.)

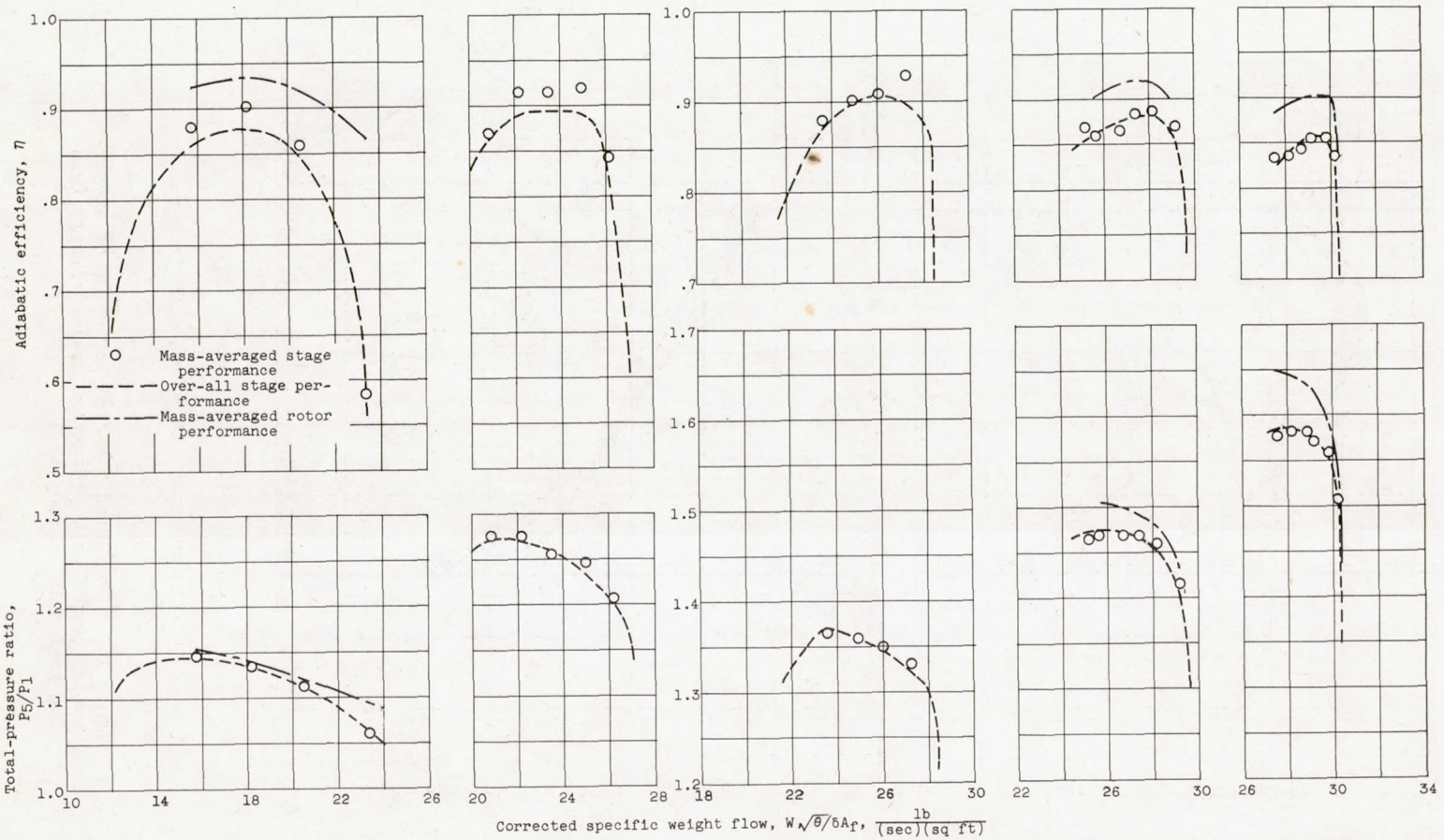


(a) Corrected rotor tip speed, 600 feet per second.

(b) Corrected rotor tip speed, 800 feet per second.

(c) Corrected rotor tip speed, 900 feet per second.

(d) Corrected rotor tip speed, 1000 feet per second.

(e) Corrected rotor tip speed, 1100 feet per second.

Figure 16. - Stage-performance characteristics.

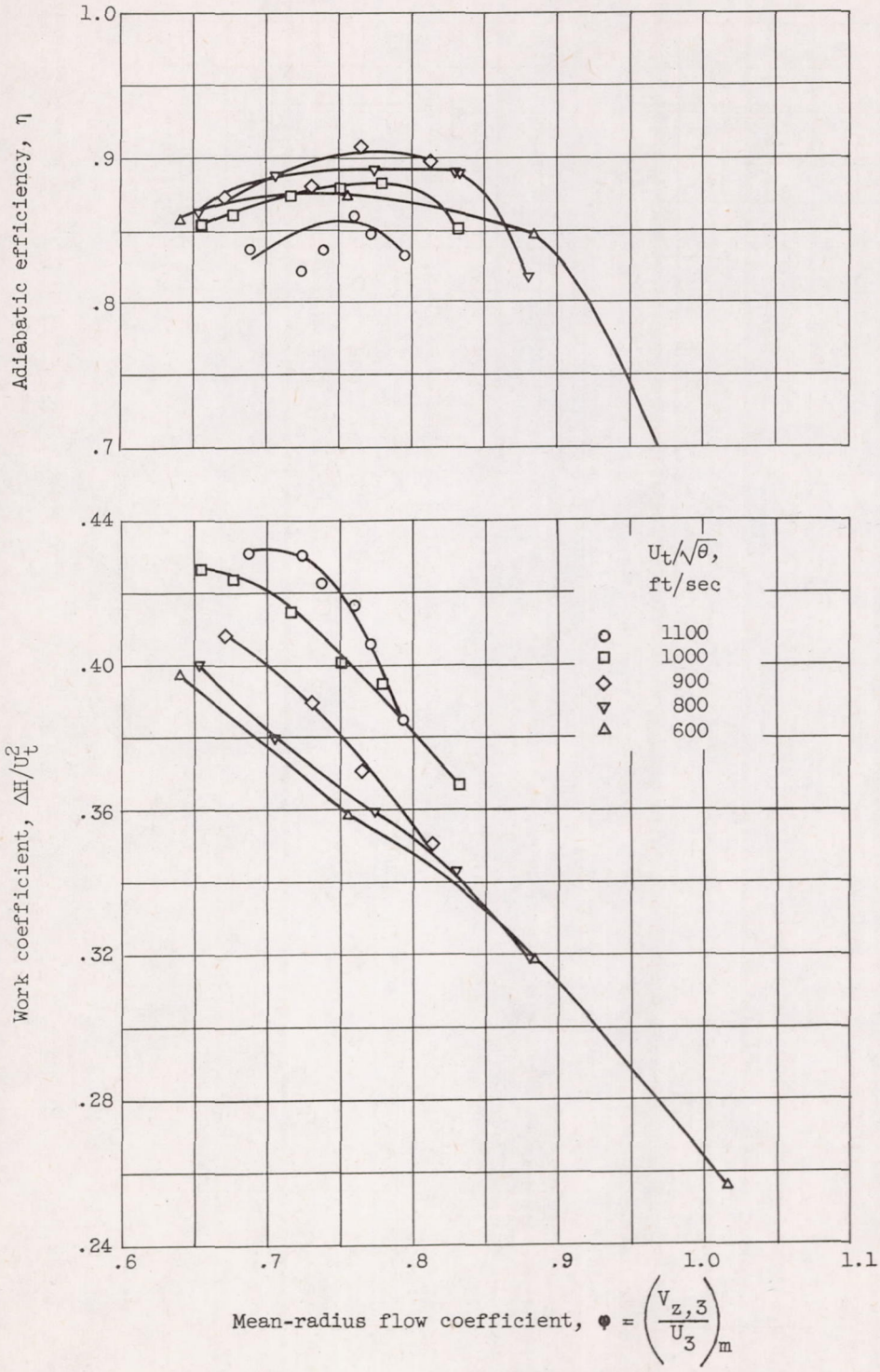


Figure 17. - Variation of stage over-all adiabatic efficiency and work coefficient with flow coefficient.